Geosci. Model Dev. Discuss., 3, 1–59, 2010
www.geosci-model-dev-discuss.net/3/1/2010/

Geoscientific Model Development Discussions

This discussion paper is/has been under review for the journal Geoscientific Model Development (GMD). Please refer to the corresponding final paper in GMD if available.

Implementation and evaluation of a new methane model within a dynamic global vegetation model: LPJ-WHyMe v1.3

R. Wania[1,*], I. Ross[2,], and I. C. Prentice[3]**

[1]Department of Earth Sciences, University of Bristol, Wills Memorial Building, Queen's Road, Bristol, BS8 1RJ, UK
[2]School of Geographical Sciences, University of Bristol, University Road, Bristol BS8 1SS, UK
[3]QUEST, Department of Earth Sciences, University of Bristol, Wills Memorial Building, Queen's Road, Bristol, BS8 1RJ, UK
[*]now at: School of Earth and Ocean Sciences, University of Victoria, P.O. Box 3055, Victoria, BC, V8W 3V6, Canada
[**]now at: Mathematics and Statistics, University of Victoria, P.O. Box 3060 STN CSC, Victoria, BC, V8W 3R4, Canada

Received: 8 December 2009 – Accepted: 15 December 2009 – Published: 15 January 2010

Correspondence to: R. Wania (rita@wania.net)

Published by Copernicus Publications on behalf of the European Geosciences Union.

Abstract

For the first time, a model that simulates methane emissions from northern peatlands is incorporated directly into a dynamic global vegetation model. The model, LPJ-WHyMe (LPJ-*W*etland *Hy*drology and *Me*thane), was previously modified in order to simulate peatland hydrology, permafrost dynamics and peatland vegetation. LPJ-WHyMe simulates methane emissions using a mechanistic approach, although the use of some empirical relationships and parameters is unavoidable. The model simulates methane production, three pathways of methane transport (diffusion, plant-mediated transport and ebullition) and methane oxidation. Two sensitivity tests were conducted, first to identify the most important factors influencing methane emissions and secondly to justify the choice of parameters. A comparison of model results to observations from seven sites revealed in general good agreement but also highlighted some problems. Circumpolar methane emissions for the period 1961–1990 were estimated to be between 40.8 and 73.7 Tg CH_4 a^{-1}.

1 Introduction

Wetlands are the largest individual source of methane (CH_4) emissions and contribute 100–231 Tg CH_4 a^{-1} to a global budget of 582 Tg CH_4 a^{-1} (Denman et al., 2007). Peatlands are one type of wetland that occurs mainly in the boreal and arctic regions but can also be found in tropical areas such as Indonesia or in tropical alpine regions. Northern peatlands cover an area of approximately 3.0–3.2×10^6 km^2 north of 40° N (Matthews and Fung, 1987; Aselman and Crutzen, 1989). Zhuang et al. (2004) summarised the current literature and found that emission estimates for the pan-arctic region from eleven studies ranged from 31 to 106 Tg CH_4 a^{-1}. A recent inverse modelling study allocated only 33±18 Tg CH_4 a^{-1} of total global emissions to northern wetlands (Chen and Prinn, 2006).

Even though present-day methane emissions from northern wetlands contribute only about 5–18% of global annual, natural and anthropogenic, methane emissions (this

estimate is based on northern wetland CH_4 emissions by Zhuang et al. (2004) and global CH_4 emissions found in Denman et al., 2007) their relative contribution may increase under future climate change that will increase temperature and precipitation in the high latitude regions faster and more than in other regions on Earth (Meehl et al., 2007; Christensen et al., 2007). However, the processes that underlie methane emissions are complex and depend on variables such as inundation, vegetation composition, and soil temperature. These variables interact with one other, and temperature and precipitation changes in the future may have positive or negative feedback effects on wetland methane emissions.

Methane emissions to the atmosphere result from a balance between CH_4 production and CH_4 oxidation. Methane is produced by methanogens which are obligate anaerobic archaea, which means that they require oxygen-free environments (Vogels et al., 1988; Whitman et al., 1992). The three most important factors influencing the level of activity of methanogens and therefore CH_4 production rates are the degree of anoxia, the temperature, as microbes increase their activity level up to a threshold temperature after which the activity level declines again (Svensson, 1984), and the availability of suitable carbonaceous substrate that can be utilised. Once CH_4 is produced, it can be transported to the atmosphere via diffusion through the peat pore water, it can be transported through the gas-filled pore spaces (aerenchyma) of vascular plants or it can be released abruptly in the form of bubbles.

Before methane escapes to the atmosphere, it may be oxidised by methanotrophic bacteria that utilise CH_4 as a carbon and energy source (Hanson and Hanson, 1996). In peatlands, methanotrophs are aerobic bacteria and their activity therefore depends on the amount of oxygen available in the peat. Oxygen can either diffuse into the peat pore water from the surface (Benstead and Lloyd, 1996) or it can be transported to the tips of the roots of vascular plants, leading to high CH_4 oxidation rates (Ström et al., 2005). It is crucial to account for both oxygen transport mechanisms when modelling CH_4 oxidation.

In order to study methane emissions from northern peatlands, a process-based modelling approach that takes account of interactions between vegetation, hydrology, soil thermal regime and methane-related processes is needed. In the past, methane models have been developed to estimate methane emissions from global wetlands (Cao et al., 1996; Walter and Heimann, 2000; Zhuang et al., 2004), but these models did not include the dynamic interactions between hydrology, soil temperature, vegetation and methane processes. A review of previous methane models can be found in Wania (2007). Here, we describe a new methane model that is integrated into a dynamic global vegetation model and which takes the interactions mentioned above into account. The aim of this study is to show how LPJ-WHyMe reproduces observed data when simulating CH_4 emissions, without the use of site-specific input data. We discuss the uncertainties that arise and the difficulties of modelling CH_4 emissions.

2 Model description

2.1 LPJ-WHyMe

LPJ-WHyMe is a development of the Lund-Potsdam-Jena Dynamic Global Vegetation Model (LPJ) originally described in Sitch et al. (2003) and Gerten et al. (2004). LPJ is a processed-based model that describes plant physiology, carbon allocation, decomposition and hydrological fluxes in terms of mathematical equations. Vegetation is defined by plant functional types (PFTs) that group plants with similar traits together. Each PFT is described by allocating specific parameters that distinguish one PFT from another. PFTs thus function differently under different environmental conditions and compete for resources such as light and water. This competition determines the simulated vegetation composition.

LPJ-WHyMe stands for LPJ-*W*etland *Hy*droglogy and *Me*thane emissions and was originally described in Wania (2007). LPJ-WHyMe is a further development of LPJ-WHy, which dealt with the introduction of permafrost and peatlands into LPJ (Wania

et al., 2009a). Implementing peatlands in LPJ-WHy required the addition of two new PFTs (flood-tolerant C_3 graminoids and *Sphagnum* mosses), the introduction of inundation stress for non-peatland PFTs, a slow-down in decomposition under inundation and the addition of a root exudates pool (Wania et al., 2009b).

2.2 Methane model structure

The addition of a methane model did not require any changes to the rest of the model as the development of LPJ-WHy was targeted towards later inclusion of a methane model. A separate subroutine containing the methane model was simply added to the program. All of the input variables required to drive the methane model were already available. This feature distinguishes LPJ-WHyMe from other methane modelling approaches, where output from vegetation models that took no account of changes in vegetation due to inundation were used to drive methane models, neglecting the potential effects of changes in vegetation composition, reduction in net primary production and the deceleration of decomposition (e.g., Cao et al., 1996; Walter et al., 2001).

The basic concept of the methane model in LPJ-WHyMe is that a "potential carbon pool for methanogens" is created (Fig. 1). This "potential carbon pool for methanogens" is distributed over all soil layers, weighted by the root distribution (Fig. 2, top). This carbon is then split into CO_2 and CH_4 (Fig. 2, bottom). Based on the amount of CH_4 available in each layer, the dissolved CH_4 concentration and the gaseous CH_4 fraction are calculated. Part of the CH_4 is oxidised by oxygen that has diffused into the soil layer or has been transported through plants to the soil layer. After the oxidation is determined, dissolved methane can be transported to the atmosphere either by diffusion or through plant tissue (aerenchyma). Gaseous CH_4 can escape to the atmosphere by ebullition. The sum of ebullition, diffusion and plant-mediated transport represents the total CH_4 flux from the soil to the atmosphere. All of the processed mentioned above are described in detail in subsequent sections.

2.2.1 Potential carbon pool for methanogenesis

The carbon pool available for methanogenic archaea consists mainly of root exudates and easily degradable plant material, and to a much lesser extent material from the decomposition of more recalcitrant organic matter (Chanton et al., 1995). A root exudates pool was introduced into LPJ-WHy (Wania et al., 2009b) as a very labile carbon pool with a fast turnover rate k_{exu}. The exudates pool is directly linked to net primary production, with a fixed fraction, f_{exu}, of net primary production being diverted into the exudates pool at each timestep. LPJ-WHyMe models the decomposition of above- and belowground litter, at rate k_{litter}, and of the fast and the slow soil carbon pools, at rates k_{fast} and k_{slow}, respectively (Fig. 1). Decomposition rates are a function of soil temperature (R_T), which follows Lloyd and Taylor (1994) and of soil moisture content (R_{moist}) via empirically fitted relationships (Wania et al., 2009b, Sect. 2.3):

$$k = k^{10} R_T R_{\mathrm{moist}}, \tag{1}$$

where k represents the turnover rates for exudates, litter, and the fast and slow carbon pools, and k^{10} the respective decomposition rates at 10 °C (Table 1). The moisture response, R_{moist}, is chosen so that the decomposition rate is reduced under inundation. The carbon resulting from this decomposition is classified as heterotrophic respiration in LPJ, but in LPJ-WHyMe, we treat this carbon differently at peatland and non-peatland sites. At non-peatland sites the pool behaves in exactly the same way as in LPJ and is immediately added to the atmospheric carbon dioxide flux. For peatland sites, the decomposed carbon is put into the potential carbon pool available to methanogens.

2.2.2 Root distribution

Carbon from the potential carbon pool for methanogenesis is allocated to each soil layer according to the root biomass distribution. For the hydrology part it was sufficient to split the root biomass between acrotelm and catotelm, but for modelling the carbon cycle within the soil, a more detailed root distribution is required to allocate carbon to

each 0.1 m thick soil layer, and also to estimate the plant-mediated transport of oxygen and methane into and out of each layer. The root distribution used in LPJ-WHyMe is based on data from six cores from a transition fen, a blanket bog and a raised bog in Wales, UK (Gallego-Sala, 2008) and from a detailed analysis of three different species from three micro-sites in western New York, USA (Bernard and Fiala, 1986). Gallego-Sala did not separate dead from living roots and it is therefore unclear whether all roots she found in the top one metre of soil should be counted as living biomass. However, Saarinen (1996) noted that living roots of *Carex rostrata* Stokes can be found to a depth of 2.3 m. The root distribution based on Gallego-Sala and Bernard and Fiala's data shows an exponential decrease of root biomass with depth which is fitted as

$$f_{\text{root}} = C_{\text{root}} e^{z/\lambda_{\text{root}}}, \quad (2)$$

where f_{root} is the fraction of root biomass at the level under consideration, z is the vertical coordinate, positive upwards, i.e. negative values are below the surface, λ_{root}=25.17 cm is the decay length and C_{root}=0.025 is a normalisation constant to give a total root biomass of 100% within 2 m depth. This dependence is used for the flood-tolerant C_3 graminoid plant functional type in LPJ-WHyMe. The acrotelm (i.e. the top 0.3 m) contains around 60% of root biomass, which means that the majority of available C occurs in the acrotelm. When soil layers are permanently frozen throughout the year, the root biomass from the frozen layer is moved upwards to the first unfrozen layer.

2.3 Methane and carbon dioxide production

Under anaerobic conditions, decomposition rates are slower than under aerobic conditions, leading to the accumulation of organic material. The decomposed carbon is mainly turned into carbon dioxide, but a fraction is reduced to methane. The molar ratio of methane production to carbon dioxide production varies from 0.001 to 1.7 in anaerobic conditions (Segers, 1998). In a previous methane modelling approach, methane/carbon dioxide (CH_4/CO_2) ratios of 0.0001 to 0.1 were used, depending on the water table position (Potter et al., 1996). These wide ranges make it clear that the

methane/carbon dioxide ratio is difficult to predict, mainly because other electron acceptors, such as NO_3^-, Mn^{4+}, Fe^{3+} or SO_4^-, are reduced before methane is produced (Segers, 1998). We therefore elect to treat the methane/carbon dioxide ratio as an adjustable parameter in LPJ-WHyMe. The ratio is currently set to 0.25 under full inundation and is weighted by the degree of anoxia, α, defined as $\alpha = 1 - f_{\text{air}}$, where f_{air} is the fraction of air in each layer. The air fraction can be derived by using the soil porosity, the volumetric fractions of mineral and organic material and the fraction of water and ice, all of which are calculated in the soil temperature subroutine (Wania et al., 2009a, Sect. 2.1.2). A similar approach was used by Segers and Leffelaar (1996), who calculated P_{CH_4}, the methane production rate, as $P_{CH_4} = ICF$, where I is an aeration inhibition function (I=1 under anoxic conditions, I=0 under oxic conditions), C is the anaerobic carbon mineralisation rate and F is the fraction of the anaerobically mineralised carbon that is transformed into methane.

2.4 Methane oxidation

Knowing how much oxygen reaches each soil layer via diffusion and plant-mediated transport (described below), we can estimate how much methane is oxidised at each time step. Two assumptions need to be made:

(i) Part (25%) of the oxygen is utilised either by the roots themselves or by non-methanotrophic microorganisms. At the moment, we assume that 75% of oxygen is available to methanotrophic bacteria;

(ii) This means that 75% of the oxygen is used to oxidise methane. Stoichiometric balance requires two moles of oxygen for each mole of methane oxidised:

$$CH_4 + 2O_2 \rightarrow CO_2 + 2H_2O. \quad (3)$$

We assume that if enough oxygen is available, all of the methane is oxidised. If less oxygen is available than required, then all of the oxygen is used up in oxidising methane. Oxidised methane is added to the carbon dioxide pool.

In Sect. 4 we test the sensitivity of methane emissions to the oxygen availability fraction parameter and adjust its value accordingly.

2.5 Diffusion processes

Since diffusion of gases in the soil column is governed by essentially the same equation as temperature variations, we use the same Crank-Nicolson numerical scheme as in Wania et al. (2009a, Supplementary Text S1 and Fig. S1) to solve the diffusion equation for gas transport via molecular diffusion within the soil. This is straightforward when the gas diffusivities are known. Gas diffusion processes occur more quickly than heat diffusion so require a shorter time step. The time step in the Crank-Nicolson scheme is set to one hundredth of a day (about 15 min).

A more difficult aspect of modelling gas diffusion is setting up boundary conditions at the water-air interface. At the water-air boundary, gas diffusivities change by at least four orders of magnitude. One approach would be to use the conventional Fick's law relation:

$$J = -D\frac{(C_{\text{water}} - C_{\text{air}})}{\Delta z}, \tag{4}$$

where J is the gas flux, D is the mean gas diffusivity in water and air, assuming that the air layer on top is of the same thickness as the soil layer, C_{water} and C_{air} are the gas concentrations in water and air and Δz is the soil layer thickness. Because of the far greater diffusivity in air, the mean diffusivity will be heavily biased towards the diffusivity in air, thus will be relatively large and lead to large fluxes out of the water into the air. The only way to solve Eq. (4) would be to specify the thickness of the air layer that contributes significantly to the gas flux. If the air layer were thin, it would be possible to approximate the flux J. This approach seems unsatisfactory as there is no way to approximate the air layer thickness without more detailed information. A more robust way to calculate the flux from the top layer (saturated or unsaturated soil) into

the overlying air layer is as

$$J = -\psi(C_{\text{surf}} - C_{\text{eq}}), \tag{5}$$

where C_{surf} is the concentration of gas measured in the surface water, and C_{eq} is the equilibrium concentration of gas in the atmosphere (McGillis et al., 2000). The gas exchange coefficient, ψ, with units of velocity, is termed the piston velocity, which is "the height of the water that is equilibrated with the atmosphere per unit time for a given gas at a given temperature" (Cole and Caraco, 1998). A way to estimate the piston velocity ψ for different gases is to relate it to the known, measured, piston velocity of a different substance, in this case SF_6. We can calculate the piston velocity of another gas, $\psi_\bullet$, as

$$\psi_\bullet = \psi_{600}\left(\frac{Sc_\bullet}{600}\right)^n, \tag{6}$$

where

$$\psi_{600} = \left(2.07 + 0.215 \times U_{10}^{1.7}\right)c \tag{7}$$

is the piston velocity (in m s^{-1}) of SF_6 normalised to a Schmidt number[1] of 600 (dependent on the wind speed in 10 m height, U_{10}, in m s^{-1}), $Sc_\bullet$ is the Schmidt number of the gas in question, and $n = -\frac{1}{2}$ (Riera et al., 1999). The constant c has the value 36 and serves to convert ψ_{600} to SI units of m s^{-1}. Using Eq. (6), the piston velocities for methane, carbon dioxide and oxygen may then be calculated.

Ideally, the wind speed would be used to force LPJ-WHyMe, but there are two issues here. One is that the CRU TS 2.1 climate data set does not include wind speeds. The other issue is that one would need to know the wind speed in the peatland vegetation, not just above the vegetation canopy, as the exchange of air within the vegetation is important to drive the concentration gradients of gases. However, the water-atmosphere

[1] The Schmidt number, Sc, of a gas is the ratio between the coefficient of momentum diffusivity, i.e. the kinematic viscosity, and the coefficient of mass diffusivity.

interface in peatlands is often found below the peat surface or within dense vegetation, which will reduce wind speed drastically. Therefore we assume that the wind speed within the peatland vegetation is negligible and choose to set the wind speed in LPJ-WHyMe to a constant value of $U_{10}=0\,\mathrm{m\,s^{-1}}$.

The Schmidt numbers for carbon dioxide and methane can be deduced from Jähne et al. (1987) by fitting a third-order polynomial to the observations, following Riera et al. (1999). The Schmidt number for oxygen was derived from Wanninkhof (1992). The fitted relations give

$$\begin{aligned} Sc_{\mathrm{CH_4}} &= 1898 - 110.1T + 2.834T^2 - 0.02791T^3, \\ Sc_{\mathrm{CO_2}} &= 1911 - 113.7T + 2.967T^2 - 0.02943T^3, \\ Sc_{\mathrm{O_2}} &= 1800.6 - 120.1T + 3.7818T^2 - 0.047608T^3, \end{aligned} \tag{8}$$

where T is temperature in °C.

The concentration, C_{eq}, in Eq. (5), in $\mathrm{mol\,L^{-1}}$, of a dissolved gas in equilibrium with the gas partial pressure, p_{partial}, above the solution can be estimated using Henry's law as $C_{\mathrm{eq}}=p_{\mathrm{partial}}/k_{\mathrm{H,inv}}$, where $k_{\mathrm{H,inv}}$ is Henry's coefficient in units of $\mathrm{L\,atm\,mol^{-1}}$. For methane in the atmosphere, $p_{\mathrm{partial}}=p_{\mathrm{CH_4}}=1.7\times10^{-6}$ atm. The temperature dependence of Henry's coefficient is given by

$$\log k_{\mathrm{H,inv}}(T) = \log k_{\mathrm{H}}^{\ominus} - C_{\mathrm{H,inv}}\left(\frac{1}{T} - \frac{1}{T^{\ominus}}\right), \tag{9}$$

where T is temperature in K, $k_{\mathrm{H}}^{\ominus}$ is Henry's constant at standard temperature $T^{\ominus}$, and $C_{\mathrm{H,inv}}$ is a coefficient (Sander, 1999a). Table 2 lists values and units for these parameters.

In the case of methane and carbon dioxide, the surface concentration C_{surf} will be greater than C_{eq} and J will be negative, indicating flux from the soil to the atmosphere. For oxygen, the balance will be reversed and J will be positive, indicating flux of gas into the soil.

2.5.1 Diffusivity of gases

The molecular diffusivities $D_{\mathrm{CH_4}}$, $D_{\mathrm{CO_2}}$ and $D_{\mathrm{O_2}}$ depend on temperature, the amounts of water and air in the soil and the soil porosity. We derive diffusivities in water by fitting a quadratic curve to observed diffusivities at different temperatures (Broecker and Peng, 1974), giving

$$\begin{aligned} D_{\mathrm{CH_4,water}} &= 0.9798 + 0.02986T + 0.0004381T^2, \\ D_{\mathrm{CO_2,water}} &= 0.939 + 0.02671T + 0.0004095T^2, \\ D_{\mathrm{O_2,water}} &= 1.172 + 0.03443T + 0.0005048T^2, \end{aligned} \tag{10}$$

where T is the soil temperature in °C and $D_{\bullet,\mathrm{water}}$ is the diffusivity of methane, carbon dioxide and oxygen in water in $10^{-9}\,\mathrm{m^2\,s^{-1}}$. For diffusion in air, we use values given by Lerman (1979) to find the dependence of diffusivities on the temperature:

$$\begin{aligned} D_{\mathrm{CH_4,air}} &= 0.1875 + 0.0013T, \\ D_{\mathrm{CO_2,air}} &= 0.1325 + 0.0009T, \\ D_{\mathrm{O_2,air}} &= 0.1759 + 0.00117T, \end{aligned} \tag{11}$$

where T is the soil temperature in °C and $D_{\bullet,\mathrm{air}}$ is the diffusivity of methane, carbon dioxide and oxygen in air in $10^{-4}\,\mathrm{m^2\,s^{-1}}$.

For diffusion through soil, we also need to take account of the effect of soil porosity on the diffusivity. Our estimation of the diffusivity in porous soil, $D_{\bullet,\mathrm{soil}}$, follows the Millington-Quirk model (Millington and Quirk, 1961). It has been shown by Iiyama and Hasegawa (2005) that this model gives better results for peat soils than the Three-Porosity-Model (Moldrup et al., 2004), which has only been tested for mineral soils.

Using the Millington-Quirk approach, we find

$$D_{\bullet,\mathrm{soil}} = \frac{(f_{\mathrm{air}})^{10/3}}{\Phi^2} D_{\bullet,\mathrm{air}}, \tag{12}$$

where $D_{\bullet,\mathrm{soil}}$ is the overall diffusivity of a gas in porous soil, f_{air} is the fraction of air (or the air-filled porosity as it is termed by Millington and Quirk) and Φ is the overall porosity. $D_{\bullet,\mathrm{air}}$ is the diffusivity of the respective gas in air from Eqs. (11).

For layers where $f_{\mathrm{air}} \leq 0.05$, the diffusivities for water are used. When $f_{\mathrm{air}} > 0.05$, the diffusivities in air, which are four orders of magnitude larger than those in water, become more important, and the values calculated in Eq. (12) are used. The final diffusivities, $D_{\bullet}$ are thus

$$D_{\bullet} = \begin{cases} D_{\bullet,\mathrm{water}}, & f_{\mathrm{air}} \leq 0.05, \\ D_{\bullet,\mathrm{soil}}, & f_{\mathrm{air}} > 0.05. \end{cases} \tag{13}$$

2.6 Transport through aerenchyma

The second pathway for methane and carbon dioxide to escape to the atmosphere and for oxygen to enter the soil is via transport through vascular plants. Vascular plants adapt to inundation by developing aerenchyma, gas-filled tissue in roots, rhizomes, stems and leaves. As well as their main adaptive function of delivering oxygen to the roots, aerenchyma constitute direct conduits for the transport of methane and carbon dioxide from the soil to the atmosphere. Gases transported through aerenchyma either follow a concentration gradient or are actively pumped upwards. Here, we consider only the passive flux of methane and carbon dioxide through plants as it is the most dominant form of gas transport (Cronk and Fennessy, 2001). The main factors for transport through aerenchyma are thus (i) the abundance of aerenchymatous plants; (ii) the biomass of aerenchymatous plants; (iii) the phenology of aerenchymatous plants, i.e. the period roots, stems and leaves are available for gas transport; and (iv) the rooting depth of aerenchymatous plants, which determines the depth to or from which gas can be transported.

Forbs (herbaceous plants other than grasses) can have aerenchyma, but their contribution to the overall net primary production in peatlands is generally small compared to graminoids. Dwarf shrubs, which may contribute more significantly to the net primary production than forbs, do not have aerenchyma. Therefore, forbs and dwarf shrubs were not included in LPJ-WHyMe, although we recognise that dwarf shrubs may contribute significantly to net primary production of peatlands and influence CH_4 emissions via root exudates. It is therefore desirable to include dwarf shrubs into future versions of our model.

Before methane enters the plant tissue a relatively large proportion is oxidised in the highly oxic zone around the roots, where methanotrophs thrive. Rhizospheric oxidation is species dependent and can reach 100% in *Juncus effusus* L. and *Eriophorum vaginatum* L., but can be much lower in e.g. *Carex rostrata* with 20–40% oxidation (Ström et al., 2005).

Plant-mediated transport in LPJ-WHyMe occurs solely via the flood-tolerant C_3 graminoid plant functional type, with the gas flux through vascular plants being related to the cross-sectional area of tillers[2] available to transport gas. The mass of the tillers is estimated by multiplying the leaf biomass by the daily phenology, φ:

$$m_{\mathrm{tiller}} = b_{\mathrm{leaf}}^{\mathrm{graminoid}} \varphi. \tag{14}$$

The daily phenology φ in LPJ-WHyMe describes the fraction of potential leaf cover on each day. Deciduous plant functional types have zero leaf cover in winter and build up their leaf cover over the first few growing months. Maximum leaf cover is reached after a given growing degree day threshold. The daily phenology is also influenced by drought stress. The tiller biomass m_{tiller} is then divided by the average weight of an individual tiller to obtain the number of tillers, n_{tiller}. The average observed tiller biomass

[2] Tillers are segmented stems produced at the base of many plants in the family Poaceae, with each stem possessing its own two-part leaf. The usage of the word "tiller" has been expanded to the order of Poales, which includes both groups, grasses and sedges, and is here used in its wider meaning.

for *Eriophorum angustifolium* Honckeny and *Carex aquatilis* Wahlenb. in Alaska was 0.48 g dry matter per tiller, which corresponds to 0.22 g C per tiller, assuming a C content of 45% (Schimel, 1995). The cross-sectional area of tillers, A_{tiller}, is derived by multiplying the area of an individual tiller, πr_{tiller}^2, where r_{tiller} is the tiller radius, by the number of tillers, n_{tiller} and the tiller porosity, Φ_{tiller}:

$$A_{\text{tiller}} = n_{\text{tiller}} \Phi_{\text{tiller}} \pi r_{\text{tiller}}^2 . \quad (15)$$

A first estimate of the tiller radius, r_{tiller}, was derived by averaging over the two widespread species *Eriophorum angustifolium* (3.95 mm) and *Carex aquatilis* (1.9 mm) (Schimel, 1995), yielding r_{tiller}=2.9 mm. The tiller porosity is initially set to 50% (Cronk and Fennessy, 2001). Schimel (1995) also measured *E. scheuchzeri* Hoppe whose tillers contained only 0.09 g dry matter and whose tiller radius was 0.85 mm. Using these values to calculate the tiller cross-sectional area gives a similar value to that based on our values above (0.48 g dry matter and 2.9 mm radius) for the same biomass. In Sect. 4, the sensitivity of methane emissions to the tiller radius and porosity is tested.

Finally, each layer is allocated a fraction of the total cross-sectional area of tillers according to the respective root fraction in that layer.

2.7 Ebullition

It has been shown that methane bubble formation is initiated well below saturation levels (Baird et al., 2004). Before Baird et al.'s study, models assumed that dissolved methane concentration had to reach 7.1 to 8.0 mg CH_4 L^{-1}, i.e. 40–45% of saturation levels, before bubbles could form. However, Baird et al.'s experimental studies revealed that bubble formation started at around 3.5% saturation. These new findings were taken into account in the design of this model, i.e. gaseous methane in bubble form exists at all times. The amount of gaseous methane depends on the overall methane concentration and Henry's Law, which tells us how much methane occurs in dissolved and how much in gaseous form. In other models, dissolved methane accumulates first

and bubble formation occurs only above a relatively high concentration (>500 µMol) of dissolved methane (Walter et al., 1996).

2.7.1 Gaseous vs. dissolved methane

From Henry's Law, we know that a gas dissolved in a liquid is in equilibrium with the partial pressure of that gas. We can thus use the gaseous methane concentration to derive the concentration of dissolved methane in the pore water. For this purpose, we use a definition of Henry's Law in terms of concentrations, namely

$$k_{\text{H}}^{cc} = c_{\text{a}} / c_{\text{g}} \quad (16)$$

where k_{H}^{cc} is the dimensionless ratio of aqueous concentration, c_{a}, to gaseous concentration, c_{g}. Henry's constant, k_{H}, in mol L^{-1} atm^{-1}, the inverse of $k_{\text{H,inv}}$ from Eq. (9), is given by

$$k_{\text{H}} = 1 / k_{\text{H,inv}} . \quad (17)$$

Further, k_{H}^{cc} can be related to k_{H} using a relationship from Sander (1999a,b):

$$k_{\text{H}}^{cc} = T k_{\text{H}} / 12.2 , \quad (18)$$

where T is in Kelvin. This allows us to calculate c_{a}

$$c_{\text{a}} = k_{\text{H}}^{cc} c_{\text{g}} . \quad (19)$$

Assuming that methane is first produced in the gaseous phase and subsequently dissolves in the pore water (previous modelling approaches have worked in the opposite sense, computing dissolved methane concentration first and then deriving the concentration of gaseous methane), the amount of dissolved methane can be estimated by substituting c_{g} in Eq. (19) by the total methane concentration, C_{CH_4}, in the soil layer. However, this will give the concentration of dissolved methane in equilibrium with the *total* methane concentration C_{CH_4}, where $c_{\text{a}}+c_{\text{g}}>C_{CH_4}$ as $c_{\text{g}}=C_{CH_4}$. We

therefore subtract c_a from C_{CH_4}, so that $c_a+c_g=C_{CH_4}$. Ideally, one would iterate this approximation until the true equilibrium is reached. For now we keep in mind that we slightly overestimate the amount of dissolved methane. This possible overestimation is minor compared to uncertainties in the carbon pool calculation and methane production processes.

An upper limit on the quantity of dissolved methane is imposed, with the maximum solubility of methane at a given temperature following Yamamoto et al. (1976). The best-fit curve through Yamamoto et al.'s observations is

$$S_B = 0.05708 - 0.001545T + 0.00002069T^2, \quad (20)$$

where S_B is the Bunsen solubility coefficient, defined as volume of gas dissolved per volume of liquid at atmospheric pressure and a given temperature. We use the ideal gas law to convert the volume of methane per volume of water into moles as

$$n = pV/RT, \quad (21)$$

where $p=p_{atm}+\rho gz$ is the sum of the atmospheric and hydrostatic pressures (Pa), calculated from the density of water (ρ), acceleration due to gravity (g) and water height (z), V is the methane volume (m^3), T is the temperature (K), the gas constant R is 8.3145 m^3 Pa K^{-1} mol^{-1} and n is the amount of gas (mol). Atmospheric pressure has been shown to be a trigger for ebullition (Tokida et al., 2007), but atmospheric pressure is not yet used as an input variable for LPJ-WHyMe and is therefore assigned a constant value.

2.7.2 Ebullition threshold

Once the methane concentration for each layer is known, the volumetric gas content is calculated. Typical values for volumetric gas contents in experiments and in the field are 12–15%, above which most ebullition events occur (Kellner et al., 2005; Strack et al., 2005; Baird et al., 2004). Therefore, if the volumetric gas content, VGC, in LPJ-WHyMe exceeds the maximum volumetric gas content threshold VGC_{max} of 15%,

ebullition occurs from that layer with the amount of methane escaping to the atmosphere being the amount by which the volume of methane exceeds the lower limit of the volumetric gas content, VGC_{low}. VGC_{low} can be set to be the same as VGC_{max}, in which case only the excess methane escapes at each time step. This leads to frequent releases of methane of a relatively small volume. If we assume that once an ebullition event is triggered more methane than just the excess over the minimum VGC escapes, the VGC will drop below VGC_{max}. Hence, if we set $VGC_{low}<VGC_{max}$ we will have less frequent, but larger releases of methane. The amount of methane released per year will be almost identical in each case for a given temperature and pressure. VGC_{low} can therefore be seen as a tuning factor for the frequency and amplitude of ebullition. The gas liberated by ebullition is assumed to escape to the atmosphere immediately. The simulation of ebullition takes account of the methane content in gas bubbles, found on average to be about 57% of total gas content (Kellner et al., 2006).

3 Evaluation sites and experimental setup

3.1 Input data for LPJ-WHyMe

Input data needed to drive LPJ-WHyMe are climate data and atmospheric CO_2 concentrations. Soil texture information is not required as all grid cells for which LPJ-WHyMe is run are set to the organic soil type. For the site-by-site comparison we used the Climate Research Unit time series data CRU TS 2.1 (Mitchell and Jones, 2005). This data set provides monthly air temperature and cloud cover, monthly total precipitation and monthly number of wet days from 1901–2002. The time series data were used to permit effective comparison of individual model years to observations. Atmospheric carbon dioxide concentrations for 1901–2002 were taken from Etheridge et al. (1996) and Keeling and Whorf (2005). For model spin-up, the first 10 years of the CRU data were repeated until 1000 years of spin-up time had been completed. Potential problems with this spin-up procedure for peatlands are discussed in Wania et al. (2009b).

3.2 Observations

The sites used for sensitivity studies and model evaluation are summarised in Table 3.

3.2.1 Site 1: Michigan, USA

The Buck Hollow Bog is located in southern Michigan and is classified as an ombrotrophic peatland covered by a wet lawn of *Sphagnum* species and densely vegetated by *Scheuchzeria palustris* L., a rush (Shannon and White, 1994). Other vascular species include cranberries (*Vaccinium oxycoccus* L.), cottongrass (*Eriophorum virginicum* L.) and a leatherleaf dwarf shrub (*Chamaedaphne calyculata* (L.) Moench) (Shannon and White, 1994). Methane fluxes were measured at three sites representing the wet *Sphagnum-S. palustris* lawn micro-habitat. Mean annual temperature over 1961–1990 was 8.2 °C and mean annual precipitation was 778 mm at the nearby weather station in Lansing, Michigan (http://www.nrcc.cornell.edu).

3.2.2 Site 2: Minnesota, USA

The Minnesota site is located in the US Forest Service Marcell Experimental Forest. Methane flux data from Junction Fen are used for the model-data comparison. Junction Fen is a poor fen which receives some runoff from the surrounding uplands; lacking an outlet, it is wetter than nearby peatland sites. Vegetation is dominated by a sedge (*Carex oligosperma* Michaux) with some rush (*Scheuchzeria palustris*) and cranberry (*Vaccinium oxycoccus*). The graminoids grow above a peat moss mat composed of *Sphagnum angustifolium* (C. Jens. ex Russ) C. Jens., *S. capillifolium* (Ehrh.) Hedw. and *S. fuscum* (Schimp.) Klinggr. Mean annual temperature (1961–1990) is 3 °C and mean annual precipitation is 770 mm (Dise, 1993).

3.2.3 Site 3: BOREAS Northern Study Area, Canada

The BOREAS Northern Study Site is located in central Manitoba near Thompson, and is a fen site with vegetation consisting of a variety of peat mosses (*Sphagnum* spp.), brown moss species (*Drepandocladus exannulatus* (B.S.G.) Warnst.), the bog-bean (*Menyanthes trifoliata* L.) and sedges (*Carex* spp.) (Joiner et al., 1999). The sparse overstorey consists of larch (*Larix laricina* (Du Roi) K. Koch) and bog birch (*Betula glandulosa* Michx.) (Joiner et al., 1999). Methane fluxes from several micro-sites are available for the Collapse Fen and Zoltai Fen (Bubier et al., 1998) and were used here. Mean January temperature is −25.0 °C and mean July temperature is 15.7 °C; mean annual precipitation is 536 mm (Gower et al., 2001).

3.2.4 Site 4: Salmisuo, Finland

The Salmisuo mire complex is situated in Eastern Finland and consists of a minerogenic, oligotrophic low-sedge *Sphagnum papillosum* (Lindb.) pine fen (Saarnio et al., 1997). Methane fluxes from both lawn micro-sites were used for our study. The lawn habitats are vegetated by cottongrass (*Eriophorum vaginatum* L.), with bog-rosemary (*Andromeda polifolia* L.), cranberry (*Vaccinium oxycoccus*) and a sedge (*Carex pauciflora* Lightf.). The moss layer is dominated by *S. angustifolium* (Russow) C. Jens., *S. balticum* (Russow) C. Jens., with some *S. magellanicum* Brid. and *S. papillosum* Lindb. (Saarnio et al., 1997). Mean annual air temperature (1971–2000) is 2.0 °C, with temperatures in January of −11.9 °C and in July of 15.8 °C; mean annual precipitation is 600 mm (Alm et al., 1999).

3.2.5 Site 5: Degerö, Sweden

The Degerö Stormyr is part of the Kulbäcksliden Research Park in Västerbotten county in Sweden and is about 70 km from the Gulf of Bothnia (Granberg et al., 2001b). Methane data were collected in the poor fen community which is dominated by

cottongrass (*Eriophorum vaginatum*), cranberry (*Vaccinium oxycoccus*), bog-rosemary (*Andromeda polifolia*), rush (*Scheuchzeria palustris*), and a sedge (*Carex limosa* L.). The moss layer is dominated by *Sphagnum balticum*, *S. majus* (Russ.) C. Jens. and *S. lindbergii* Schimp. in Lindb. (Granberg et al., 2001a). Mean annual temperature (1961–1990) is 2.3 °C, with temperatures in January of −12.4 °C and in July of 14.7 °C; mean annual precipitation is 523 mm (Granberg et al., 2001b).

3.2.6 Site 6: Abisko, Sweden

The subarctic Stordalen mire is part of the Abisko research area in Northern Sweden. Since 2006, methane fluxes have been recorded using an eddy-covariance flux tower. These half-hourly methane data provide a high-resolution data set for this site. The flux tower covers a wet part of the palsa mire with cottongrass (*Eriophorum vaginatum*) and a moss (*Drepanocladus* sp.) as dominant species. The peat is underlain by permafrost with a maximum active layer depth of about 70–80 cm for the period 2000–2002 (Christensen et al., 2004). The mean annual air temperature (1913–2003) in Abisko, which lies 10 km west of Stordalen, is −0.7 °C with temperatures in January of −10.9 °C and in July of 11.6 °C; mean annual precipitation is 304 mm (Johansson et al., 2006).

3.2.7 Site 7: Ruoergai, China

The Ruoergai plateau lies on the eastern edge of the Qinghai-Tibetan plateau at 3400 m altitude. The peatland area on the Qinghai-Tibetan plateau is estimated to exceed 32 000 km^2, constituting 45% of China's wetlands and 75% of China's peatlands (Ding et al., 2004). Methane emissions from the Qinghai-Tibetan plateau peatlands are estimated to be around 0.45 Tg CH_4 a^{-1} (Ding et al., 2004). The peatland on the Ruoergai Plateau is dominated by two sedges, *Carex meyeriana* Kunth. and *C. muliensis*. Mean annual temperature is 1 °C with a minimum temperature of −10.7 °C in January and maximum temperature of 10.3 °C in July; mean annual precipitation is 650 mm (Ding et al., 2004).

This site is included in our study as a representative of high altitude peatlands, for comparison with the behaviour of high latitude peatlands. Although our focus here is on the high latitudes, we can thus provide an initial evaluation of the suitability of LPJ-WHyMe for the simulation of methane fluxes from such high altitude environments.

Note: the CRU mean annual temperature for the grid cell corresponding to the Ruoergai study site, with coordinates 32°47′ N, 102° 32′ E, deviated from the observed climate by +3 °C. We suspect that this is due to the steep topography in this region, where a small error in location may lead to a large change in climate. To compensate for this effect, we therefore use the adjacent grid cell to the west, which has a mean annual temperature of 1.4 °C (minimum −10.5 °C, maximum 11.4 °C, for the period 1998–2002). These values are similar to the observed climate and are expected to provide a better fit of model results to observed methane fluxes.

3.3 Vegetation and land surface processes

Net primary production simulated by LPJ-WHyMe (Table 4), soil temperature and water table position (Fig. 3) are presented to provide a framework for the interpretation of methane emission results. Total net primary production ranges from 276 to 478 g C m^{-2} a^{-1}, which includes both aboveground and belowground net primary production. A discussion of these simulated net primary production values can be found in Wania et al. (2009b). The percentage of *Sphagnum* moss net primary production ranges from 0–23% of total net primary production, which means that flood-tolerant C_3 graminoids are the dominant PFT in terms of net primary production.

Permafrost occurs at the BOREAS, Abisko and Ruoergai sites, because soil temperatures in deeper soil layers never rise above 0 °C (Fig. 3). Since the BOREAS and Abisko sites lie in the zone of discontinuous permafrost, it is not unrealistic for LPJ-WHyMe to simulate permafrost conditions.

All sites but Ruoergai show a snow melt peak at the beginning of the growing season resulting in the highest water table positions at the Salmisuo and Abisko sites. Wania et al. (2009a) deals with the evaluation of the simulation of soil temperature and

water table position in LPJ-WHyMe in detail – we present these results here to provide context for the ensuing discussion of methane flux results.

4 Sensitivity test I

4.1 Method

An initial sensitivity experiment was performed for eight parameters, assessed as being the most uncertain and potentially having the most influence on methane emissions. The parameters used are listed in Table 5 and the values used in each sensitivity experiment are shown in Table 6.

The sensitivity results were summarised by regressing the different methane fluxes, i.e. plant-mediated, diffusion, ebullition, and total flux, against each set of parameter values. Fluxes were normalised by the maximum of each flux type for each site to enable comparison of regression slopes between sites and flux types.

4.2 Results and discussion

Total methane flux as well as plant-mediated transport, diffusive flux and ebullition were used to evaluate the importance of each of the eight parameters varied in this experiment. Results are summarised in Fig. 4. The parameters on the left hand side plus the top parameter on the right hand side in Fig. 4 influence the production or oxidation of methane, while the other three parameters affect methane transport pathways. Values use for each parameter are listed in Table 6.

Methane/carbon dioxide ratio, CH_4/CO_2

The results show that the most important parameter for all fluxes is the ratio of methane to carbon dioxide production under anaerobic conditions, CH_4/CO_2. As expected,

higher CH_4/CO_2 leads to greater methane emissions. Plant-mediated transport increases least, while ebullition increases most, probably because the capacity for plant-mediated transport is limited and quickly saturates, so that additional methane escapes via ebullition and diffusion.

Oxidation fraction, f_{oxid}

The greater the fraction of available oxygen used for the oxidation of methane, f_{oxid}, the less methane is emitted. The strongest reductions are seen in the diffusive fluxes, as diffusion happens only from the top soil layer, which has the highest oxygen concentrations and is where most methane oxidation takes place. Plant-mediated transport and ebullition are also affected because oxygen is transported down to deeper soil layers via aerenchyma, where it leads to decreased methane concentrations.

Fraction of exudates, f_{exu}

The fraction of exudates has a small effect in both directions. Both increases and decreases in methane fluxes are seen at sites 1, 3, 4 and 5, while sites 2, 6 and 7 show only negative correlations with increasing f_{exu}. The effect of increasing f_{exu} is complex: higher f_{exu} values will lead to more exudates being available for methane production, but f_{exu} is subtracted from the net primary production and therefore decrease net primary production, which can lead to an overall negative effect on methane emissions.

Exudate turnover rate, k_{exu}

Changes in the decomposition rate of exudates, k_{exu}, produced little effect on any of the fluxes, which suggests that there is enough carbon in the heterotrophic respiration pool to supply carbon for methanogenesis in each soil layer.

Moisture response, R_{moist}

The moisture response, R_{moist}, used to calculate decomposition rates, had a small positive effect on almost all methane fluxes. Higher R_{moist} values led to faster turnover times, which increased the availability of carbon and enhanced CH_4 emissions slightly.

Tiller porosity, Φ_{tiller}

The tiller porosity is used in Eq. (15) and influences the area available for plant-mediated transport. Higher porosity values lead to a slight increase in total emissions at five sites, whereas plant-mediated transport was enhanced at all sites, leading to a reduction in the other two flux categories. Not only does enhanced plant-mediated transport reduce CH_4 concentrations in the pore water, it also increases oxygen transport to the roots and increases CH_4 oxidation.

Tiller radius, r_{tiller}

The tiller radius is used in the same equation as the tiller porosity, i.e. Eq. (15). A larger tiller radius has a similar effect on plant-mediated transport to tiller porosity as it increases gas diffusion through plants. The sensitivity test shows that the range of parameter values chosen for the tiller radius (see Table 6) influences the balance between plant-mediated transport and ebullition more than the tiller porosity. Plant-mediated transport shows a much stronger increase and ebullition a much stronger decrease when tiller radius is varied than when the tiller porosity is varied. The effect on the total methane flux is weaker and similar to the impact of varying leaf-to-root ratio or tiller porosity.

Volumetric gas content limit, VGC_{low}

By modifying the volumetric gas content range between its lower limit, VGC_{low}, and the threshold for ebullition, VGC_{max}, we can alter the amount of methane released

by each individual ebullition event and also the frequency with which ebullition events occur. Lower VGC_{low} values lead to less frequent ebullition events with larger amplitudes, while higher VGC_{low} values produce more frequent ebullition with smaller amplitude events. As explained in Sect. 2.7.2, the lower limit of the volumetric gas content, VGC_{low}, determines the quantity of methane that escapes to the atmosphere at each ebullition event. The more methane that escapes in a single event, the longer it will take to build up enough methane to trigger another ebullition event. The annual total of ebullition fluxes is not influenced by the value used for VGC_{low}. When VGC_{low} is set to the same value as VGC_{max}, the threshold above which ebullition occurs, the total flux curve is very smooth as a small amount of methane escapes almost every day during the growing season.

4.3 Conclusions

Sensitivity tests revealed that the parameters with the greatest influence on total methane emissions were the ratio of methane to carbon dioxide production under anaerobic conditions and the fraction of oxygen used by methanotrophs. The methane to carbon dioxide ratio is used to determine the fraction of heterotrophic respiration that is transformed into methane. This ratio is fixed but is weighted by the air fraction in each layer, an indicator of the degree of anoxia in that layer. This ratio has a linear influence on overall methane fluxes, because as more carbon is allocated to methane, more methane is available in the soil and so methane fluxes are higher. Experimental studies to determine the ratio of methane to carbon dioxide production show good agreement with our choice of parameter value (Gallego-Sala, 2008).

The second parameter, the fraction of oxygen used by methanotrophs, f_{oxid}, also has a direct and linear influence on methane concentrations and therefore on methane fluxes. The parameter f_{oxid} determines how much of the dissolved oxygen in the soil is used by methane-oxidising bacteria and how much is used by the respiration of other microorganisms. This means that for higher values of f_{oxid}, more methane will be oxidised. However, if more oxygen is used for methane oxidation, less oxygen is

available for heterotrophic respiration and therefore less carbon dioxide is produced. This means that a possible way to improve our knowledge of f_{oxid} in the future is to evaluate carbon dioxide emissions together with methane emissions while balancing the stoichiometry of carbon dioxide, methane and oxygen.

5 Sensitivity test II and model-observation data comparison

5.1 Method

The results of sensitivity test I were used to design a second sensitivity experiment. The only parameter not included in this second sensitivity test was VGC_{low} as it had little influence on methane fluxes and is purely a tuning factor for the frequency and amplitude of ebullition events. For the second sensitivity experiment, we used only three values per parameter (see right hand side of Table 6), but this time, we ran the model for all of the possible 2187 different combinations in the parameter space. The daily results were summarised as average daily fluxes per month. Histograms of these average daily fluxes per month were used to present the range and frequency of methane emissions generated based on the chosen parameter values.

A best guess set of parameters was chosen subjectively, based on visual comparison of fit between model results with varying parameters and observations, for daily as well as total annual methane emissions. The paucity of methane emission data – only 60% of mean monthly observations were based on more than two daily observations – made it difficult to apply statistical methods to compare mean monthly simulated emissions to mean monthly observations. The chosen set of parameters was used for all of the seven test sites. Parameters could be tuned to individual sites to improve the match between observations and model, which may be desirable if LPJ-WHyMe was applied to study methane dynamics at a specific site. However, since one of the goals of this study was to develop a circumpolar methane model that can be applied for large areas for which we do not have any data available to tune the model, we used the same set

of parameters for all sites here to show how well LPJ-WHyMe performs using a single set of parameters.

5.2 Results and discussion

Methane emissions from seven sites resulting from sensitivity test II are compared to results based on our best guess parameter values and to observations (Fig. 5). The best guess parameters are listed in Table 6. Figure 5 shows that the best guess simulation (black line) lies more or less in the middle of the histogram data, which indicates that the combination of parameters chosen for the best guess do not result in any extreme minimum or maximum results. Below, we discuss the results in detail for each site.

Michigan

LPJ-WHyMe captures the methane emissions occurring between January and April and between August and December well, but misses out on the high emissions during the summer months. The failure to simulate high summer emissions may partially be caused by the lack of ebullition at this site (Table 7), due to a combination of factors. When we compare the Michigan site to the Minnesota site, which shows ebullition (Table 7), we notice the following differences: Despite Michigan having a lower annual net primary production than Minnesota, it has a higher flood-tolerant C_3 graminoid leaf biomass (105 vs. 50 g C m^{-2}). The lower annual net primary production at the Michigan site is caused by a combination of higher root biomass (263 vs. 126 g C m^{-2}) and higher soil temperatures (10.1 vs. 4.3 °C in 25 cm depth) that lead to a higher overall maintenance respiration, which reduces productivity more at the Michigan site than at the Minnesota site. The lower net primary production leads to slightly lower CH_4 concentrations in the soil and the volumetric gas content (VGC_{max}) threshold set for ebullition is not reached. The contribution of CH_4 emissions transported through plants is higher at the Michigan site because of the higher leaf biomass leading to

increased plant-mediated transport in both directions, i.e. transporting methane to the atmosphere and transporting oxygen down to the roots. Both lead to reduced concentrations of dissolved and gaseous methane and can therefore explain the absence of ebullition events.

The estimated observed plant-mediated flux for the dominant species *Scheuchzeria palustris* at this site is about 250 mg CH_4 m^{-2} d^{-1} (Shannon et al., 1996), which is slightly above the peak values shown in Fig. 5. Shannon et al. (1996) estimated the contribution of *S. palustris* to the total methane emissions to be between 64 and 90%, whereas LPJ-WHyMe simulates 99% plant-mediated emissions, hinting at an underestimation of ebullition and/or diffusive fluxes by LPJ-WHyMe. Modelled annual methane flux is 31.9 g CH_4 m^{-2} a^{-1}. Observations for the two temperate bogs at this site ranged from 0.2 to 47.3 g CH_4 m^{-2} a^{-1} for Big Cassandra Bog and from 66.9 to 76.3 g CH_4 m^{-2} a^{-1} for Buck Hollow Bog (Shannon and White, 1994). The modelled value lies in the range of Big Cassandra Bog.

Minnesota

The Minnesota site shows good agreement between observations and simulated methane fluxes in all months but June (Fig. 5). Daily peak values in July are reproduced by ebullition events in LPJ-WHyMe, which are smoothed out in the plot, but the model does not simulate emissions that match the monthly average value of over 500 mg CH_4 m^{-2} d^{-1} in July. The histogram in Fig. 5 shows that the model does not achieve high enough CH_4 emissions in June with any of the parameter combinations considered. The modelled reduction in CH_4 emissions in June coincides with a drop in water table position (Fig. 3), which is the likely reason why LPJ-WHyMe cannot simulate CH_4 emissions that match the observations. This reduction in methane emissions due to a drop in water table is seen in June rather than later on in the summer because soil decomposition increases with higher temperatures and thus so do CH_4 production rates, compensating for the lower water table position.

Plant-mediated transport and ebullition contributed about equally to about 90% of the total annual CH_4 emissions of 46.1 g CH_4 m^{-2} a^{-1} (Table 7), which compares well to the observed range of 3.2 to 65.7 g CH_4 m^{-2} a^{-1} (Dise, 1993).

BOREAS

Model results for the BOREAS site are generally lower than the observed fluxes (Fig. 5), but the overall observed pattern is represented by the model. Some of the observed values lie within the values of the histogram, indicating that some combinations of parameters can reproduce these higher methane fluxes. When comparing the modelled CH_4 fluxes to the observed monthly averaged daily fluxes (stars), the only month with a really large deviation between the two is July. An interesting feature of the histogram is that it shows discontinuous values, e.g. from October to December. This discontinuity is caused by ebullition, which is defined by gas concentration thresholds in LPJ-WHyMe. Once the threshold is reached, the emissions jump discontinuously from one level to a higher one.

For the BOREAS site, plant-mediated transport was the most important flux with 56.4% of total emissions, while ebullition contributed most of the remainder, as diffusion was as small source of CH_4. Total simulated methane emissions were 21.1 g CH_4 m^{-2} a^{-1}. Unfortunately, we do not have an observed estimate of annual CH_4 emissions from this site.

Salmisuo

Observations at the Salmisuo site are well matched by model results over the entire year (Fig. 5) and the histogram covers almost all of the data points. LPJ-WHyMe produces slightly excessive CH_4 emissions in June, July and October. All of the observed high daily values in mid-summer can be matched by simulated ebullition events.

CH_4 fluxes at the Salmisuo site, together with those at the Degerö site, are dominated by ebullition, which accounts for 62.8% at the Salmisuo site. This dominance

can be explained by the highest net primary production values but a lower percentage of flood-tolerant C_3 graminoids than the Michigan, Minnesota and BOREAS sites (Table 7). The lower percentage of flood-tolerant C_3 graminoids will decrease the plant-mediated transport of CH_4 out of the soil and oxygen into the soil. Gaseous CH_4 can therefore accumulate and cause ebullition. Total annual simulated emissions were $58.0\,g\,CH_4\,m^{-2}\,a^{-1}$. Observations for the period 1 June to 17 October 1993 estimate the fluxes to be 30.4 and $36.8\,g\,CH_4\,m^{-2}\,a^{-1}$ for an *Eriophorum* and a *Carex* lawn, respectively (Saarnio et al., 1997). The LPJ-WHyMe emissions for the same period are $38.2\,g\,CH_4\,m^{-2}\,a^{-1}$.

Degerö

The Degerö site shows an overestimation of CH_4 fluxes in almost all months (Fig. 5). The most likely reason for this disparity is the exclusion of ebullition events from the observed data, as samples with anomalously high methane concentrations were rejected (Granberg et al., 2001a,b). If only diffusive and plant-mediated methane fluxes are compared to observations, the modelled results are much closer to the observations (data not shown). Plant-mediated transport at the Degerö site contributes 38.1% to the total, diffusion 4.6% and ebullition 57.2%. Another modelling study arrived at similar results, namely a joint contribution of diffusion and ebullition of 6–48% (Granberg et al., 2001a). The observed range of methane emissions for May to September for the years 1995–1997 is 16, 13 and $18\,g\,CH_4\,m^{-2}$, respectively (Granberg et al., 2001a). The simulated annual plant-mediated and diffusive flux in our study is $17.5\,g\,CH_4\,m^{-2}\,a^{-1}$ in 1996 and $13.4\,g\,CH_4\,m^{-2}\,a^{-1}$ for May to September 1996, which closely matches the observations.

Abisko

The Abisko/Stordalen site is the only site for which we used data from an eddy-covariance flux tower. Figure 5 shows that LPJ-WHyMe is able to reproduce values

similar to observations in the first half of the year, but simulated values plateau in summer and decrease too early in autumn. The rather abrupt decrease of CH_4 emissions in August is due to the way that LPJ models leaf phenology. When the air temperature drops below the growing degree day minimum of 5 °C, leaves of deciduous PFTs are shed. The air temperatures used to drive LPJ-WHyMe are realistic and the timing of the simulated leaf shedding in August corresponds to the observed leaf senescence in 2006 and 2007 (Jackowicz-Korczyński et al., 2010). Therefore, we believe that the general model setup in LPJ is realistic and useful. However, for our CH_4 modelling framework, this sudden leaf shedding means that plant-mediated transport is suddenly cut off. This points towards a problem in LPJ-WHyMe: in the real world, methane may escape through plants even after they have died, as tillers usually constitute a passive conduit for CH_4 transport (Cronk and Fennessy, 2001), and their transport system should remain functioning at least for a while after leaf senescence. This does not happen in the model so far and it may be necessary to include this process into a future version of LPJ-WHyMe. Another reason for the lower simulated summer emissions may be that LPJ-WHyMe simulates frequent ebullition events during the time when most of the pore water is frozen. The way that LPJ-WHyMe is currently set up permits ebullition as long as there is some liquid water in the relevant soil layer. This may not be fully accurate as frozen layers at the soil surface may inhibit any bubble release and this may influence CH_4 emissions later in the year. However, high methane emissions have been observed during times when soil water is freezing (Mastepanov et al., 2008) and ebullition events in autumn or winter may therefore be justifiable, as simulated by LPJ-WHyMe and visible at the BOREAS and Abisko sites in Fig. 5 (in the form of a ragged black line for the best-guess simulations or non-continuous histogram plots).

Plant-mediated transport contributed 80.4% to total methane emissions and ebullition was responsible for 19.0%. Total annual simulated CH_4 emissions were $16.3\,g\,CH_4\,m^{-2}\,a^{-1}$ (Table 7), which is lower than the observed 22.9–$27.2\,g\,CH_4\,m^{-2}\,a^{-1}$. We doubt that this underestimation is caused by the comparison of different years, i.e., the model year 2002 versus the observed year 2006. It is more

likely that the dependence of plant mediated transport on living plant tissue is the culprit.

Ruoergai

LPJ-WHyMe captures some of the observed pattern of methane fluxes at the Ruoergai site, although the simulated data do not show a seasonality as strong as the observations (Fig. 5). Discontinuity in the histogram plots shows that ebullition events are very common. The model using the best-guess parameters overestimates some of the emissions but the observations are widely spread from June to September and the model results lie within the range of observations.

Ding et al. (2004) estimated mean methane fluxes for the two different *Carex* species at the Ruoergai site to be 2.06 and 3.88 mg CH_4 m^{-2} h^{-1} and the average growing season length to be 165 days. This results in observed fluxes of 8.2 and 15.3 g CH_4 m^{-2} a^{-1}, only about half of the 29.0 g CH_4 m^{-2} a^{-1} simulated by LPJ-WHyMe. One reason for the higher modelled fluxes could be that LPJ-WHyMe models net primary production of 352 g C m^{-2} a^{-1} (Table 4), which equates to 782 g m^{-2} a^{-1} dry mass (45% carbon content), relatively high compared to the observed net primary production of 285–750 g m^{-2} a^{-1} dry mass. Plant-mediated transport and ebullition contributed equally to the total, while diffusion was small (Table 7).

6 Circumpolar methane emissions

6.1 Methods

The Climate Research Unit climatology data set CL 1.0 (New et al., 1999) was used to drive LPJ-WHyMe for the circumpolar region. This data set provides monthly air temperature and cloud cover, monthly total precipitation and monthly number of wet days averaged over the years 1961–1990. Atmospheric CO_2 concentration was set

to a constant 321 ppm, representing the mean value over the 20th century. Note that there is no need to prescribe atmospheric CH_4 concentrations for our simulations. The model was spun up for 1000 model years and run for 1 year thereafter at a resolution of 1°×1°. In order to provide methane emissions suitable for comparison with other studies and observations, it is advantageous to scale the outputs of LPJ-WHyMe to account for two factors.

The first factor to consider is the overall area of peatlands simulated in our model as compared to other studies. A map of fractional peatland cover was produced, based on organic soil carbon content derived from the IGBP-DIS 5′×5′ resolution map (Global Soil Data Task Group, 2000)[3]. The resulting peatland area between 45° N and 90° N is 5.37×10^6 km^2, a value that exceeds other estimates (Matthews and Fung, 1987; Aselman and Crutzen, 1989; Prigent et al., 2007). This overestimate of peatland area will lead to concomittant overestimates in CH_4 emissions. The estimated maximum area of bogs and fens in Russia, Europe, Canada and Alaska is $2.99–3.20\times10^6$ km^2 (Matthews and Fung, 1987; Aselman and Crutzen, 1989). To correct for these differences, we will scale CH_4 emissions from LPJ-WHyMe accordingly. We find scaling factors of 0.56–0.60 (by dividing Matthews and Fung and Aselman and Crutzen's estimate by the IGBP-DIS estimate), respectively, which we define as the Matthews and Aselman scaling factors. The first multiple satellite approach to map global wetlands gives an area of approximately 1.6×10^6 km^2 for the latitudinal band of 55° N to 70° N (Prigent et al., 2007). The peatland area in the 55° N to 70° N using the IGBP-DIS data gives 4.18×10^6 km^2. The Prigent scaling factor is therefore 0.38.

The second factor to consider is the effect of peatland micro-topography. The micro-topography in peatlands is generally composed of drier sites (hummocks) and wetter sites (hollows, lawns and pools) with the drier sites having a methane emission rate of about a third to a half of that at the wetter sites (Kettunen et al., 2000; Saarnio et al., 1997). LPJ-WHyMe simulates methane emissions that lie in the range found in lawns,

[3]Details on how this map was created and the map itself can be found in Wania et al. (2009a).

which occupy around 50% of the area of typical peatlands (Alm et al., 2006; Becker et al., 2007). Based on these observations, we assume that half of the peatland area is wet and emits methane at full capacity while the other half of the area emits at 30–50% of the full capacity, leading to an overall reduction of methane emissions by 25–35%, i.e. scaling factors of 0.65–0.75.

6.2 Results and discussion

Modelled methane emissions from peatlands between 45° N and 90° N for the period 1961–1990 are shown in Fig. 6. The left-hand panel (Fig. 6a) expresses methane emissions as mean daily fluxes per m^2 per year, whereas the right-hand panel (Fig. 6b) shows total annual methane emissions per grid cell. Daily methane emissions range from zero in peatlands in the farthest north to over 250 mg CH_4 m^{-2} d^{-1} in the UK and Ireland. The CH_4 fluxes observed at two peatland sites in nearby Michigan were 11.5–209 mg CH_4 m^{-2} d^{-1}, averaged over a three year period (Shannon and White, 1994) and methane fluxes observed at a northern Minnesota peatland were 10–180 mg CH_4 m^{-2} d^{-1} (Dise, 1993), which shows that the CH_4 emissions simulated by LPJ-WHyMe are not unreasonable.

The range of methane emissions from LPJ-WHyMe is comparable to the model results of Walter et al. (2001), which showed fluxes below 100 mg CH_4 m^{-2} d^{-1} for most far northern peatlands with only a few regions in Eastern Europe reaching values between 100 and 200 mg CH_4 m^{-2} d^{-1}. The model of Zhuang et al. (2004) showed mean daily CH_4 emissions averaged over the year of 109 mg CH_4 m^{-2} d^{-1} and above. Cao et al. (1996)'s model resulted in latitudinally averaged CH_4 emissions of 120.5, 51.2, 31.6 and 12.1 mg CH_4 m^{-2} d^{-1} for the latitudinal bands of 40° N–50° N, 50° N–60° N, 60° N–70° N and 70° N–80° N, respectively. The comparable emissions from LPJ-WHyMe are 100, 73.9, 60.6 and 19.9 mg CH_4 m^{-2} d^{-1}, respectively. LPJ-WHyMe shows a less steep gradient from lower to higher latitudes and higher average emissions than Cao et al. (1996) in the three more northern latitudinal bands.

A noticeable difference between LPJ-WHyMe and the models of Walter et al. (2001) and Zhuang et al. (2004) is that LPJ-WHyMe shows a consistent latitudinal gradient in methane emissions, with emissions decreasing from south to north (Fig. 6a), whereas the other two models show a reversed trend in at least some areas (e.g. the Western Siberian Lowlands).

In LPJ-WHyMe the latitudinal gradient in emissions can be explained by the correlation between methane emission (E) in g CH_4 m^{-2} a^{-1} and soil temperature at 25 cm depth in °C (T_{25}) ($E = 27.7 + 1.87 T_{25}$, $r^2 = 0.55$, $p < 0.001$) or methane emissions and net primary production (NPP) in g C m^{-2} a^{-1} ($E = -13.96 + 0.11\,\mathrm{NPP}$, $r^2 = 0.65$, $p < 0.001$), where soil temperatures and net primary production are also correlated ($\mathrm{NPP} = 356.7 + 13.40 T_{25}$, $r^2 = 0.55$, $p < 0.001$). In Walter et al.'s study, it appears that the positive south to north gradient in the Western Siberian Lowlands, i.e. the opposite trend to LPJ-WHyMe, is caused by lower water table positions in the south in August and November, which lead to higher methane oxidation (Walter et al., 2001, Plate 2). Higher simulated oxidation rates in the south could explain why methane emissions were lower there than further north despite higher temperatures and presumably higher net primary production. The methane emission pattern in Zhuang et al. (2004) is harder to interpret. A possible explanation could be the use of soil-water pH to suppress methane emissions outside a pH range of 5.5–9.0. This pH range unrealistically excludes methane emissions from bogs, whose pH is usually below 5.5 (Siegel, 1998), potentially leading to an underestimation of methane emissions in some areas; more than half of the wetlands in Russia and Canada are bogs (Aselman and Crutzen, 1989).

Figure 6b shows CH_4 emissions per grid cell per year, weighted by the Prigent scaling factor of 0.38 and the micro-topography scaling factor of 0.75. The pattern of methane emissions changes slightly compared to Fig. 6a as areas with a high fractional peatland cover will produce more CH_4 per grid cell than other areas. The map in Fig. 6b suggests that the areas with the highest CH_4 emissions are the Hudson Bay Lowlands in Canada and Southern Scandinavia.

7 Annual budget

Applying the area and micro-topography correction factors of Sect. 6 to methane emissions from LPJ-WHyMe yields a value for the total annual methane emissions for the 45° N–90° N circumpolar region of between 40.8 and 73.7 Tg CH_4 a^{-1} for the period 1961–1990, which is in the range of previous studies. Zhuang et al. (2004) summarised the current literature and found that emission estimates for the pan-arctic region from eleven studies ranged from 31 to 106 Tg CH_4 a^{-1}. A recent inverse modelling study allocated only 33±18 Tg CH_4 a^{-1} of total global emissions to northern wetlands (Chen and Prinn, 2006), which is lower than our estimate. However, LPJ-WHyMe simulates CH_4 emissions from "natural potential vegetation" and may therefore overestimate present day CH_4 emissions. Many peatlands have been drained or destroyed, although the organic soil carbon content may still be high enough to classify the grid cell as peatland. LPJ-WHyMe will therefore run its peatland hydrology, simulating high water table positions and with it CH_4 emissions. However, drained peatlands produce little or no CH_4.

Another reason why the estimate of Chen and Prinn (2006) should be lower than the results from LPJ-WHyMe is that inverse modelling approaches such as Chen and Prinn used calculate the net flux of CH_4, i.e. CH_4 emissions minus CH_4 uptake by soils. Methane uptake by soils is estimated to be 6.9 Tg CH_4 a^{-1} for the cool temperate, boreal and polar region together (Curry, 2009), which when added to Chen and Prinn's 33±18 Tg CH_4 a^{-1} gives a range of 21.9–57.9 Tg CH_4 a^{-1}.

8 Conclusions

This is the first time that a methane emission model has been completely integrated into a dynamic global vegetation model, drawing all of its necessary input data from the vegetation model, which itself requires only climate data, atmospheric CO_2 concentration and fractional peatland cover as input. The advantage of this setup is that

the model can be applied to any point in the circumpolar region without requiring site-specific data. However, the model output can only be as good as the model inputs. We are using monthly averaged data to drive LPJ-WHyMe, but compare daily model output to observations, mainly due to the lack of monthly observations. The use of monthly average air temperature or precipitation may lead to a lack of extreme values that in reality would cause high daily CH_4 emissions, for example through ebullition events. This means that our comparison of simulated daily CH_4 emissions to observed daily emissions should be treated cautiously. One approach to this comparison issue would be to drive the model with daily meteorological data from sites where methane fluxes were measured by eddy-covariance, which provide a continuous time series of methane emissions.

LPJ-WHyMe differs from other models (Cao et al., 1996; Walter and Heimann, 2000; Zhuang et al., 2004) in several aspects (a detailed analysis of different methane models can be found in Wania, 2007). The usage of a Q10 value for CH_4 production rates is avoided by only applying a modified Arrhenius-type dependence on temperature to soil respiration (Lloyd and Taylor, 1994). We make the assumption that methanogenesis is limited by temperature only indirectly by the availability of substrate, which is linked to soil respiration in LPJ-WHyMe. We also avoid the use of Michaelis-Menten coefficients, as these can show high variability between sites (Walter and Heimann, 2000) and are therefore of little use when applying the model to many grid cells in the circumpolar region for which no observations are available. Further, we think that it is more important to know how much substrate is available, rather than the speed at which that substrate will be turned over assuming that all of the substrate is being utilised at some point.

Given these constraints, LPJ-WHyMe is able to produce good results when comparing observations from seven sites to model results. Daily, monthly and annual CH_4 emissions are all in acceptable ranges. The estimates of total circumpolar CH_4 emissions from peatlands lie within the range of previously reported CH_4 emissions (although this range is wide). The two main uncertainties in the total emissions budget

arise from the still poorly known distribution of wetlands and variations in the fractional wetland cover in each grid cell, and the variation in CH_4 emissions due to spatial heterogeneity in peatlands. Improvements in terms of peatland distribution may be made in the near future with the help of more and new remote sensing data. Advances in accounting for the influence of peatland micro-topography may be achieved using a statistical modelling approach (Rietkerk et al., 2004; Eppinga et al., 2008).

Applications of LPJ-WHyMe are far-ranging. LPJ-WHyMe can be used to simulate methane emissions from individual sites, where certain parameters could be tuned to the specific site, meteorological data from that site can be used or in- and outflow of ground water can be prescribed to improve the results. This would help to learn more about the model behaviour and potential areas for improvement. LPJ-WHyMe can be run for countries to estimate the contribution of peatlands to national greenhouse gas budgets, or it can be applied to regions for present day, future (Wania, 2007) or palaeoclimate conditions.

Acknowledgements. RW would like to thank Edward Hornibrook and Angela Gallego-Sala for inspiring discussions on model development. The authors would like to thank Nathalie de Noblet-Ducoudré, Andy Ridgwell and Paul Miller for discussion of the model setup and the manuscript. We would also like to acknowledge Cynthia A. Brewer for the provision of Colorbrewer (http://www.colorbrewer2.org). RW was sponsored by a studentship of the Department of Earth Sciences, University of Bristol, by the EU-Project HYMN (GOCE-037048) and by an NSERC Accelerator grant (34940-27346). IR was supported by a NERC e-Science studentship (NER/S/G/2005/13913).

References

Alm, J., Saarnio, S., Nykanen, H., Silvola, J., and Martikainen, P. J.: Winter CO_2, CH_4 and N_2O fluxes on some natural and drained boreal peatlands, Biogeochemistry, 44, 163–186, 1999. 20

Alm, J., Endjärv, E., Lode, E., Sillasoo, Ü., Blundell, A., Charman, D., and Karofeld, E.: Methane emissions of a bog following Late Holocene changes in water table and mire microtopography, HOLIVAR Open Science Meeting, 12–15 June 2006, UCL, London, UK Poster T4-006, 2006. 35

Aselman, I. and Crutzen, P. J.: Global distribution of natural freshwater wetlands and rice paddies, and their net primary productivity, seasonality and possible methane emissions, J. Atmos. Chem., 8, 307–358, 1989. 2, 34, 36

Baird, A. J., Beckwith, C. W., Waldron, S., and Waddington, J. M.: Ebullition of methane-containing gas bubbles from near-surface *Sphagnum* peat, Geophys. Res. Lett., 31, 299–322, 2004. 15, 17

Becker, T., Forbich, I., Schneider, J., Jager, D., Thees, B., Kutzbach, L., and Wilmking, M.: Do we miss the hot spot? The use of very high resolution imagery to quantify carbon fluxes in peatlands, Carbon in Peatlands conference, 15–18 April, 2007, Wageningen, The Netherlands, Poster, 2007. 35

Benstead, J. and Lloyd, D.: Spatial and temporal variations of dissolved gases (CH_4, CO_2, and O_2) in peat cores, Microbiol. Ecol., 31, 57–66, 1996. 3

Bernard, J. M. and Fiala, K.: Distribution and standing crop of living and dead roots in three wetland *Carex* species, B. Torrey Bot. Club, 113, 1–5, 1986. 7

Broecker, W. S. and Peng, T.-H.: Gas exchange rates between air and sea, Tellus, 26, 21–35, 1974. 12

Bubier, J. L., Crill, P. M., Varner, R. K., and Moore, T. R.: BOREAS TGB-01/TGB-03 CH_4 chamber flux data: NSA Fen. Data set. Available online [http://www.daac.ornl.gov] from Oak Ridge National Laboratory Distributed Archive Center, Tech. rep., Oak Ridge, Tennessee, USA, 1998. 20, 49

Cao, M. K., Marshall, S., and Gregson, K.: Global carbon exchange and methane emissions from natural wetlands: Application of a process-based model, J. Geophys. Res., 101, 14399–14414, 1996. 4, 5, 35, 38

Chanton, J. P., Bauer, J. E., Glaser, P. A., Siegel, D. I., Kelley, C. A., Tyler, S. C., Romanowicz, E. H., and Lazrus, A.: Radiocarbon evidence for the substrates supporting methane formation within northern Minnesota peatlands, Geochim. Cosmochim. Acta, 59, 3663–3668, 1995. 6

Chen, Y. H. and Prinn, R. G.: Estimation of atmospheric methane emissions between 1996 and 2001 using a three-dimensional global chemical transport model, J. Geophys. Res., 111, D10307, 2006. 2, 37

Christensen, J. H., Hewitson, B., Busuioc, A., Chen, A., Gao, X., Held, I., Jones, R., Kolli, R. K.,

Kwon, W.-T., Laprise, R., Rueda, V. M., Mearns, L., Menéndez, C. G., Räisänen, J., Rinke, A., Sarr, A., and Whetton, P.: Regional climate projections, in: Solomon et al. (2007), Chap. 11, 847–940, 2007. 3

Christensen, T. R., Johansson, T. R., Åkerman, H. J., Mastepanov, M., Malmer, N., Friborg, T., Crill, P., and Svensson, B. H.: Thawing sub-arctic permafrost: Effects on vegetation and methane emissions, Geophys. Res. Lett., 31, L04501, doi:10.1029/2003GL018680, 2004. 21

Cole, J. J. and Caraco, N. F.: Atmospheric exchange of carbon dioxide in a low-wind oligotrophic lake measured by the addition of SF_6, Limnol. Oceanogr., 43, 647–656, 1998. 10

Cronk, J. K. and Fennessy, M. S.: Wetland Plants: Biology and Ecology, CRC Press LLC, 2001. 13, 15, 32

Curry, C. L.: The consumption of atmospheric methane by soil in a simulated futureclimate, Biogeosciences, 6, 2355–2367, 2009, http://www.biogeosciences.net/6/2355/2009/. 37

Denman, K. L., Brasseur, G., Chidthaisong, A., Ciais, P., Cox, P. M., Dickinson, R. E., Hauglustaine, D., Heinze, C., Holland, E., Jacob, D., Lohmann, U., Rmachandran, S., da Silva Dias, P. L., Wofsy, S. C., and Zhang, X.: Couplings between changes in the climate system and biogeochemistry, in: Solomon et al. (2007), Chap. 7, 499–588, 2007. 2, 3

Ding, W. X., Cai, Z. C., and Wang, D. X.: Preliminary budget of methane emissions from natural wetlands in China, Atmos. Environ., 38, 751–759, 2004. 21, 33, 49

Dise, N. B.: Methane emission from Minnesota peatlands: spatial and seasonal variability, Global Biogeochem. Cy., 7, 123–142, 1993. 19, 30, 35

Dise, N. B., Gorham, E., and Verry, E. S.: Environmental factors controlling methane emissions from peatlands in Northern Minnesota, J. Geophys. Res., 98, 10583–10594, 1993. 49

Eppinga, M. B., Rietkerk, M., Borren, W., Lapshina, E. D., Bleuten, W., and Wassen, M. J.: Regular surface patterning of peatlands: Confronting theory with field data, Ecosystems, 11, 520–536, 2008. 39

Etheridge, D. M., Steele, L. P., Langenfelds, R. L., Francey, R. J., Barnola, J. M., and Morgan, V. I.: Natural and anthropogenic changes in atmospheric CO_2 over the last 1000 years from air in Antarctic ice and firn, J. Geophys. Res., 101, 4115–4128, 1996. 18

Gallego-Sala, A. V.: Temperature effects on trace gas production and uptake in aerobic and anaerobic soils, Ph.D. thesis, University of Bristol, 2008. 7, 26

Gerten, D., Schaphoff, S., Haberlandt, U., Lucht, W., and Sitch, S.: Terrestrial vegetation and water balance – hydrological evaluation of a dynamic global vegetation model, J. Hydrol., 286, 249–270, 2004. 4

Global Soil Data Task Group: Global gridded surfaces of selected soil characteristics (IGBP-DIS), Oak Ridge National Laboratory Distributed Active Archive Center, Oak Ridge, Tennessee, USA, http://www.daac.ornl.gov, 2000. 34

Gower, S. T., Krankina, O., Olson, R. J., Apps, M., Linder, S., and Wang, C.: Net primary production and carbon allocation patterns of boreal forest ecosystems, Ecol. Appl., 11, 1395–1411, 2001. 20

Granberg, G., Ottosson-Lofvenius, M., Grip, H., Sundh, I., and Nilsson, M.: Effect of climatic variability from 1980 to 1997 on simulated methane emission from a boreal mixed mire in northern Sweden, Global Biogeochem. Cy., 15, 977–991, 2001a. 21, 31, 49

Granberg, G., Svensson, I. S. B. H., and Nilsson, M.: Effects of temperature, and nitrogen and sulfur deposition, on methane emission from a boreal mire, Ecology, 82, 1982–1998, 2001b. 20, 21, 31

Hanson, R. S. and Hanson, T. E.: Methanotrophic bacteria, Microbiol. Rev., 60, 439–471, 1996. 3

Iiyama, I. and Hasegawa, S.: Gas diffusion coefficient of undisturbed peat soils, Soil Sci. Plant Nutr., 51, 431–435, 2005. 12

Jackowicz-Korczyński, M., Christensen, T. R., Bäckstrand, K., Crill, P., Friborg, T., Mastepanov, M., and Ström, L.: Annual cycles of methane emission from a subarctic peatland, J. Geophys. Res., doi:10.1029/2008JG000913, in press, 2010. 32, 49

Jähne, B., Heinz, G., and Dietrich, W.: Measurement of the diffusion coefficients of sparingly soluble gases in water, J. Geophys. Res., 92, 10767–10776, 1987. 11

Johansson, T., Malmer, N., Crill, P. M., Friborg, T., Åkerman, J. H., Mastepanov, M., and Christensen, T. R.: Decadal vegetation changes in a northern peatland, greenhouse gas fluxes and net radiative forcing, Glob. Change Biol., 12, 1–18, doi:10.1111/j.1365-2486.2006.01267.x, 2006. 21

Joiner, D. W., Lafleur, P. M., McCaughey, J. H., and Bartlett, P. A.: Interannual variability in carbon dioxide exchanges at a boreal wetland in the BOREAS northern study area, J. Geophys. Res., 104, 27663–27672, 1999. 20

Keeling, C. D. and Whorf, T. P.: Atmospheric CO_2 records from sites in the SIO air sampling network. In Trends: A compendium of data on global change, digital data, http://cdiac.esd.

ornl.gov/trends/co2/sio-mlo.html, 2005. 18
Kellner, E., Waddington, J. M., and Price, J. S.: 17
Dynamics of biogenic gas bubbles in peat: Potential effects on water storage and peat deformation, Water Resour. Res., 41, w08417.1–w08417.12, 2005.
Kellner, E., Baird, A. J., Oosterwoud, M., Harrison, K., and Waddington, J. M.: Effect of temperature and atmospheric pressure on methane (CH_4) ebullition from near-surface peats, Geophys. Res. Lett., 33, 397–411, 2006. 18
Kettunen, A., Kaitala, V., Alm, J., Silvola, J., Nykanen, H., and Martikainen, P. J.: Predicting variations in methane emissions from boreal peatlands through regression models, Boreal Environ. Res., 5, 115–131, 2000. 34
Lerman, A.: Geochemical processes: Water and sediment environments, John Wiley and Sons, New York, 1979. 12
Lloyd, J. and Taylor, J. A.: On the temperature dependence of soil respiration, Funct. Ecol., 8, 315–323, 1994. 6, 38
Mastepanov, M., Sigsgaard, C., Dlugokencky, E. J., Houweling, S., Strom, L., Tamstorf, M. P., and Christensen, T. R.: Large tundra methane burst during onset of freezing, Nature, 456, 628–631, 2008. 32
Matthews, E. and Fung, I. Y.: Methane emission from natural wetlands: Global distribution, area, and environmental characteristics of sources, Global Biogeochem. Cy., 1, 61–86, 1987. 2, 34
McGillis, W. R., Dacey, J. W. H., Frew, N. M., Bock, E. J., and Nelson, R. K.: Water-air flux of dimethylsulfide, J. Geophys. Res., 105, 1187–1193, 2000. 10
Meehl, G. A., Stocker, T. F., Collins, W. D., Friedlingstein, P., Gaye, A. T., Gregory, J. M., Kitoh, A., Knutti, R., Murphy, J. M., Noda, A., Raper, S. C. B., Watterson, I. G., Weaver, A. J., and Zhao, Z.-C.: Global climate projections, in: Solomon et al. (2007), Chap. 10, 747–846. 3
Millington, R. J. and Quirk, J. P.: Permeability of porous solids, Trans. Faraday Soc., 57, 1200–1207, 1961. 12, 13
Mitchell, T. D. and Jones, P. D.: An improved method of constructing a database of monthly climate observations and associated high-resolution grids, Int. J. Climatol., 25, 693–712, 2005. 18
Moldrup, P., Oleson, T., Yoshikawa, S., Komatsu, T., and Rolston, D.: Three-Porosity Model for predicting the gas diffusion coefficient in undisturbed soil, Soil Sci. Soc. Am. J., 68, 750–759, 2004. 12

New, M., Hulme, M., and Jones, P. D.: Representing twentieth century space-time climate variability. Part 1: Development of a 1961–1990 mean monthly terrestrial climatology, J. Climate, 12, 829–856, 1999. 33
Potter, C. S., Davidson, E. A., and Verchot, L. V.: Estimation of global biogeochemical controls and seasonality in soil methane consumption, Chemosphere, 32, 2219–2246, 1996. 7
Prigent, C., Papa, F., Aires, F., Rossow, W. B., and Matthews, E.: Global inundation dynamics inferred from multiple satellite observations, 1993–2000, J. Geophys. Res., 112, 305–317, 2007. 34
Riera, J. L., Schindler, J. E., and Kratz, T. K.: Seasonal dynamics of carbon dioxide and methane in two clear-water lakes and two bog lakes in northern Wisconsin, USA, Can. J. Fish. Aquat. Sci., 56, 265–274, 1999. 10, 11
Rietkerk, M., Dekker, S. C., Wassen, M. J., Verkroost, A. W. M., and Bierkens, M. F. P.: A putative mechanism for bog patterning, Am. Nat., 163, 699–708, 2004. 39
Saarinen, T.: Biomass and production of two vascular plants in a boreal mesotrophic fen, Can. J. Bot., 74, 934–938, 1996. 7
Saarnio, S., Alm, J., Silvola, J., Lohila, A., Nykänen, H., and Martikainen, P. J.: Seasonal variation in CH_4 emissions and production and oxidation potentials at microsites on an oligotrophic pine fen, Oecologia, 110, 414–422, 1997. 20, 31, 34, 49
Sander, R.: Compilation of Henry's Law Constants for inorganic and organic species of potential importance in environmental chemistry, Tech. Rep. Version 3, MPI Mainz, Air Chemistry Department, Max-Planck Institute of Chemistry, 1999a. 11, 16, 48
Sander, R.: Modeling atmospheric chemistry: Interactions between gas-phase species and liquid cloud/aerosol particles, Surv. Geophys., 20, 1–31, 1999b. 16
Schimel, J. P.: Plant transport and methane production as controls on methane flux from arctic wet meadow tundra, Biogeochemistry, 28, 183–200, 1995. 15
Segers, R.: Methane production and methane consumption: a review of processes underlying wetland methane fluxes, Biogeochemistry, 41, 23–51, 1998. 7, 8
Segers, R. and Leffelaar, P.: On explaining methane fluxes from weather, soil and vegetation data via the underlying processes, in: Northern peatlands in global climate change, edited by: Laiho, R., Laine, J., and Vasander, H., 226–241, The Academy of Finland, Helsinki, 1996. 8
Shannon, R. D. and White, J. R.: A three-year study of controls on methane emissions from two Michigan peatlands, Biogeochemistry, 27, 35–60, 1994. 19, 29, 35, 49

Shannon, R. D., White, J. R., Lawson, J. E., and Gilmour, B. S.: Methane efflux from emergent vegetation in peatlands, J. Ecol., 84, 239–246, 1996. 29

Siegel, D. I.: Evaluating cumulative effects of disturbance on the hydrologic function of bogs, fens, and mires, Env. Manag., 12, 621–626, 1998. 36

Sitch, S., Smith, B., Prentice, I. C., Arneth, A., Bondeau, A., Cramer, W., Kaplan, J. O., Levis, S., Lucht, W., Sykes, M. T., Thonicke, K., and Venevsky, S.: Evaluation of ecosystem dynamics, plant geography and terrestrial carbon cycling in the LPJ dynamic global vegetation model, Global Change Biol., 9, 161–185, 2003. 4, 47

Solomon, S., Qin, D., Manning, M., Chen, Z., Marquis, M., Averyt, K. B., Tignor, M., and Miller, H. L. (Eds.): Climate change 2007: The physical science basis. Contribution of Working Group I to the Fourth Assessment Report of the Intergovernmental Panel on Climate Change, Cambridge University Press, Cambridge, United Kingdom and New York, NY, USA, 2007. 41, 43

Strack, M., Kellner, E., and Waddington, J. M.: Dynamics of biogenic gas bubbles in peat and their effects on peatland biogeochemistry, Global Biogeochem. Cy., 19, GB1003, doi:10.1029/2004GB002330, 2005. 17

Ström, L., Mastepanov, M., and Christensen, T. R.: Species-specific effects of vascular plants on carbon turnover and methane emissions from wetlands, Biogeochemistry, 75, 65–82, 2005. 3, 14

Svensson, B. H.: Different temperature optima for methane formation when enrichments from acid peat are supplemented with acetate or hydrogen, Appl. Environ. Microb., 48, 389–394, 1984. 3

Tokida, T., Miyazaki, T., Mizoguchi, M., Nagata, O., Takakai, F., Kagemoto, A., and Hatano, R.: Falling atmospheric pressure as a trigger for methane ebullition from peatland, Global Biogeochem. Cy., 21, doi:10.1029/2006GB002790, 2007. 17

Vogels, G. D., Keltjens, J. T., and van der Drift, C.: Biochemistry of methane production, in: Biology of anaerobic microorganisms, edited by: Zehnder, A. J. B., John Wiley and Sons, New York, 707–770, 1988. 3

Walter, B. P. and Heimann, M.: A process-based, climate-sensitive model to derive methane emissions from natural wetlands: Application to five wetland sites, sensitivity to model parameters, and climate, Global Biogeochem. Cy., 14, 745–765, 2000. 4, 38, 49

Walter, B. P., Heimann, M., Shannon, R. D., and White, J. R.: A process-based model to derive methane emissions from natural wetlands, Geophys. Res. Lett., 23, 3731–3734, 1996. 16

Walter, B. P., Heimann, M., and Matthews, E.: Modeling modern methane emissions from natural wetlands 1. Model description and results, J. Geophys. Res., 106, 34189–34206, 2001. 5, 35, 36

Wania, R.: Modelling northern peatland land surface processes, vegetation dynamics and methane emissions, Ph.D. thesis, University of Bristol, 2007. 4, 38, 39

Wania, R., Ross, I., and Prentice, I. C.: Integrating peatlands and permafrost into a dynamic global vegetation model: I. Evaluation and sensitivity of physical land surface processes, Global Biogeochem. Cy., 23, GB3014, doi:10.1029/2008GB003412, 2009a. 4, 8, 9, 22, 34

Wania, R., Ross, I., and Prentice, I. C.: Integrating peatlands and permafrost into a dynamic global vegetation model: II. Evaluation and sensitivity of vegetation and carbon cycle processes, Global Biogeochem. Cy., 23, GB3015, doi:10.1029/2008GB003413, 2009b. 5, 6, 18, 22

Wanninkhof, R.: Relationship between wind-speed and gas-exchange over the ocean, J. Geophys. Res., 97, 7373–7382, 1992. 11

Whitman, W. B., Bowen, T. L., and Boone, D. R.: The methanogenic bacteria, in: The prokaryotes, a handbook on the biology of bacteria: Ecophysiology, isolation, identification, applications, 2nd edn., edited by: Ballows, A., Trüper, H. G., Dworkin, M., Harder, W., and Schleifer, K.-H., Springer-Verlag, New York, 719–767, 1992. 3

Yamamoto, S., Alcauskas, J. B., and Crozier, T. E.: Solubility of methane in distilled water and seawater, J. Chem. Eng. Data, 21, 78–80, 1976. 17

Zhuang, Q., Melillo, J. M., Kicklighter, D. W., Prinn, R. G., McGuire, A. D., Steudler, P. A., Felzer, B. S., and Hu, S.: Methane fluxes between terrestrial ecosystems and the atmosphere at northern high latitudes during the past century: A retrospective analysis with a process-based biogeochemistry model, Global Biogeochem. Cy., 18, GB3010, doi:10.1029/2004GB002239, 2004. 2, 3, 4, 35, 36, 37, 38

Table 1. Soil carbon cycle parameter values.

Parameter	Value	Units	Explanation	Reference
k_{exu}^{10}	13	a^{-1}	Exudates decomposition rate at 10 °C	Based on sensitivity analysis
k_{litter}^{10}	0.35	a^{-1}	Litter decomposition rate at 10 °C	Sitch et al. (2003)
k_{fast}^{10}	0.03	a^{-1}	Fast soil carbon pool decomposition rate at 10 °C	Sitch et al. (2003)
k_{slow}^{10}	0.001	a^{-1}	Slow soil carbon pool decomposition rate at 10 °C	Sitch et al. (2003)
f_{exu}	0.175	unitless	Fraction of NPP that is allocated to root exudates	Based on sensitivity analyses
f_{atm}	0.7	unitless	Fraction of litter fraction that is respired as CO_2	Sitch et al. (2003)
f_{fast}	0.985	unitless	Fraction of litter that enters the fast soil carbon pool	Sitch et al. (2003)
f_{slow}	0.015	unitless	Fraction of litter that enters the slow soil carbon pool	Sitch et al. (2003)

Table 2. Gas diffusion parameters taken from Sander (1999a).

Parameter	Value	Units	Description
$k_{H,inv}$	calculated	L atm mol^{-1}	Henry's coefficient
$T^{\ominus}$	298.15	K	Standard temperature
$k_H^{\ominus}$ for CH_4	714.29	L atm mol^{-1}	Henry's constant at standard temperature
for CO_2	29.41	L atm mol^{-1}	Henry's constant at standard temperature
for O_2	769.23	L atm mol^{-1}	Henry's constant at standard temperature
$C_{H,inv}$ for CH_4	1600	K	Coefficient in Henry's law
for CO_2	2400	K	Coefficient in Henry's law
for O_2	1500	K	Coefficient in Henry's law

Table 3. Sites used for sensitivity analysis and methane emissions evaluation.

No.	Site name	Country	Coordinates	Year[a]	Reference
1	Michigan	USA	42° N, 84° W	1991	Shannon and White (1994)[b]
2	Minnesota	USA	47° N, 93° W	1989	Dise et al. (1993)
3	BOREAS NSA	Canada	56° N, 99° W	1996	Bubier et al. (1998)
4	Salmisuo	Finland	63° N, 31° E	1993	Saarnio et al. (1997)
5	Degerö	Sweden	64° N, 20° E	1996	Granberg et al. (2001a)
6	Abisko	Sweden	68° N, 19° E	2006	Jackowicz-Korczyński et al. (2010)
7	Ruoergai	China	33° N, 103° E	2001	Ding et al. (2004)

[a] Year of observational data used.
[b] Data were digitised from Walter and Heimann (2000) as they plotted average values over three microsites.

Table 4. Simulated net primary production (NPP), including above- and belowground production, for the seven test sites. Net primary production is shown for the flood-tolerant C_3 graminoid PFT (ftG), *Sphagnum* moss PFT (SM) and totalled over all plant functional types (all values in g C m^{-2} a^{-1}). Note that the total net primary production equals the sum of the C_3 graminoid PFT and *Sphagnum* PFT as no other plant functional types contributed to the net primary production at these sites. The fraction of net primary production due to flood-tolerant C_3 graminoids (ftG %) is also shown.

	Michigan	Minnesota	BOREAS	Salmisuo	Degerö	Abisko	Ruoergai
ftG	273	327	261	320	291	302	260
SM	3	73	72	158	153	0	92
Total	276	400	333	478	444	302	352
ftG %	99	82	78	67	66	100	74

Table 5. Sensitivity test parameters.

CH_4/CO_2	CH_4/CO_2 production ratio under anaerobic conditions
f_{oxid}	Fraction of available oxygen used for methane oxidation
f_{exu}	Fraction of NPP put into exudates pool
k_{exu}	Turnover rate for exudates pool
R_{moist}	Moisture response, used to weight decomposition rates for exudates, litter, fast and slow carbon pools
Φ_{tiller}	Tiller porosity
r_{tiller}	Tiller radius
VGC_{low}	Lower limit of volumetric gas content

Table 6. Parameter values for initial sensitivity tests.

Parameter	Units	Sensitivity test I				Sensitivity test II			Best guess
		Value 1	Value 2	Value 3	Value 4	Value 1	Value 2	Value 3	
CH_4/CO_2	–	0.20	0.25	0.30	0.35	0.2	0.25	0.3	0.25
f_{oxid}	–	0.3	0.5	0.7	0.9	0.6	0.75	0.9	0.75
f_{exu}	–	0.05	0.10	0.15	0.20	0.10	0.15	0.20	0.175
k_{exu}	weeks	7	13	26	39	7	13	26	13
R_{moist}	–	0.2	0.3	0.4	0.5	0.2	0.35	0.5	0.35
Φ_{tiller}	%	50	60	70	80	60	70	80	70
r_{tiller}	mm	3.0	4.0	5.0	6.0	2.9	3.5	4.0	3.5
VGC_{low}	%	13.0	13.5	14.0	14.5		14.5		14.5

Table 7. Simulated plant mediated transport, diffusion, ebullition and total CH_4 fluxes ($g\,CH_4\,m^{-2}\,a^{-1}$) from seven test sites and observations taken from the references listed in Table 3. Percentage values in parentheses list the contribution of each flux type to the total flux.

No.	Site Name	Plant		Diffusion		Ebullition		Total	Observations	Notes on observations
1	Michigan	31.6	(99.0%)	0.3	(1.0%)	0	(0.0%)	31.9	0.2–47.3, 66.9–76.3	Results from 2 sites
2	Minnesota	20.7	(44.9%)	3.9	(8.5%)	21.5	(46.6%)	46.1	3.2–65.7	
3	BOREAS	11.9	(56.4%)	0.7	(3.3%)	8.5	(40.3%)	21.1		
4	Salmisuo	15.9	(27.4%)	5.7	(9.8%)	36.4	(62.8%)	58.0	9.6–40	Snow-free period only
5	Degerö	15.6	(38.1%)	1.9	(4.6%)	23.4	(57.2%)	40.9	13–18	Ebullition excluded, May–September
6	Abisko	13.1	(80.4%)	0.1	(0.6%)	3.1	(19.0%)	16.3	23.0–27.3	Eddy-covariance flux tower
7	Ruoergai	14.1	(48.6%)	0.8	(2.8%)	14.1	(48.6%)	29.0	8.2–15.3	

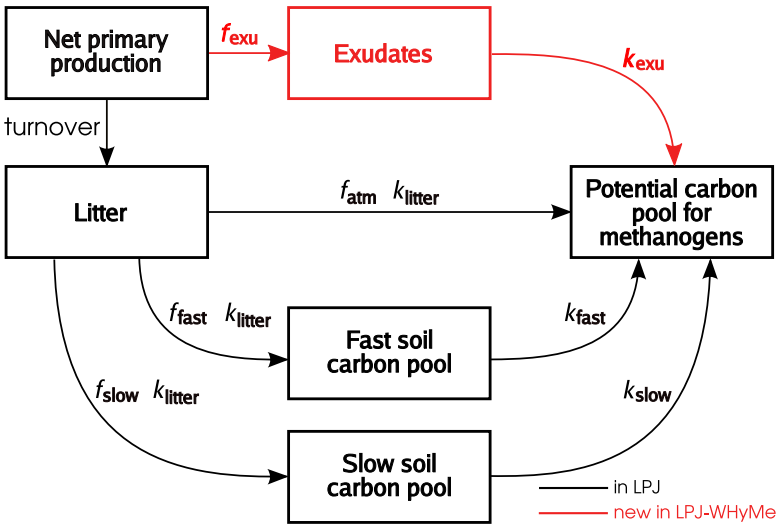

Fig. 1. Decomposition processes in LPJ-WHyMe. The turnover rate determines the fraction of net primary production converted to litter. Litter decomposes at a rate dependent on soil temperature and moisture (k_{litter}). Part of the decomposed litter (f_{atm}) goes directly into the potential carbon pool for methanogenesis; the rest is split up into the fast (f_{fast}) and the slow (f_{slow}=1−f_{fast}) soil carbon pools. Both soil carbon pools have their own temperature- and moisture-dependent decomposition rates (k_{fast}, k_{slow}). Decomposed soil carbon is added to the potential carbon pool for methanogenesis. The pathway highlighted in red indicates an addition in LPJ-WHyMe compared to the decomposition dynamics in LPJ. The fraction f_{exu} taken from the net primary production flows into an exudates pool. The decomposition rate for exudates, k_{exu}, depends again on soil temperature and moisture content. Values of various parameters are listed in Table 1.

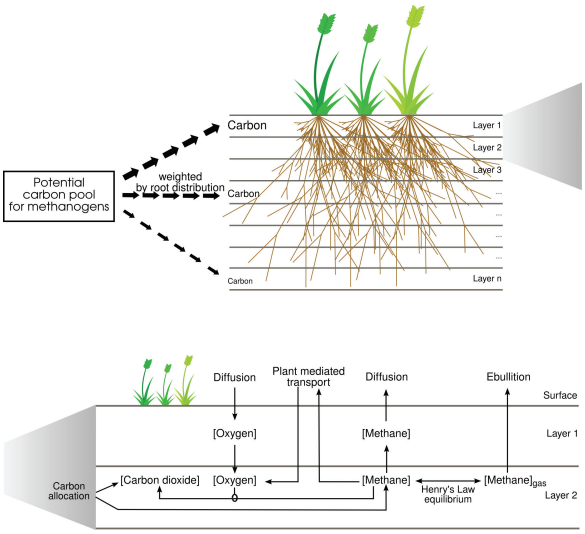

Fig. 2. Schematic representation of the LPJ-WHyMe methane model. Top: Carbon from the potential carbon pool for methanogenesis is allocated to soil layers according to the root distribution – more carbon is allocated to the upper layers where root density is greatest than to the bottom layers. Bottom: The carbon allocated to each layer is split into methane and carbon dioxide. Oxygen diffuses through the soil layers but is also transported directly from the atmosphere into the soil via vascular plants. The amount of oxygen available determines how much methane is oxidised and turned into carbon dioxide. Methane can diffuse to the atmosphere through overlying soil layers or it can escape directly to the atmosphere via vascular plants. The balance between methane in gaseous form, $[Methane]_{gas}$, and methane dissolved in pore water, [Methane], is determined using Henry's Law. If the volumetric concentration of gaseous methane reaches a threshold, an ebullition event will be triggered and methane will bubble out directly to the atmosphere.

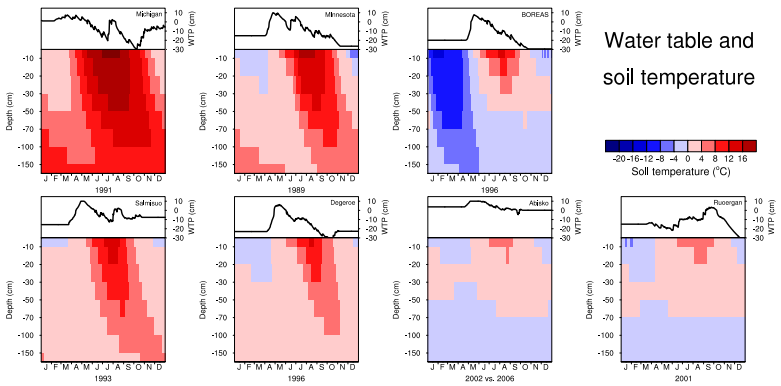

Fig. 3. Simulated water table position (line graphs) and soil temperature (contours) at the seven test sites.

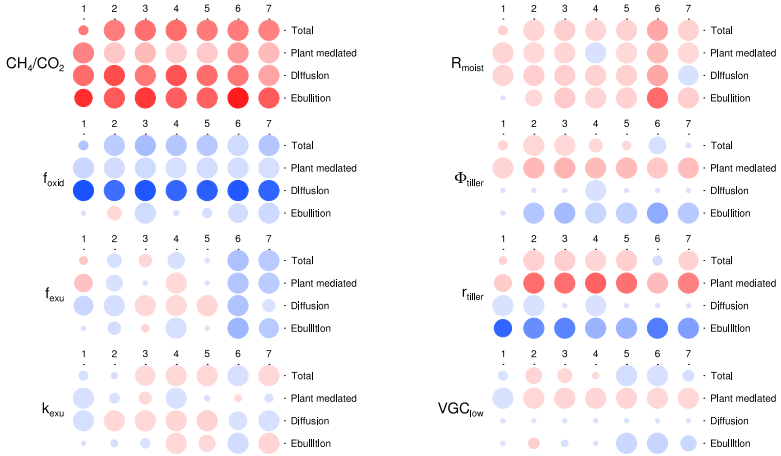

Fig. 4. Schematic summary of results of sensitivity test I. Numeric labels correspond to the site numbers in Table 3 and an explanation of the acronyms for the parameters can be found in Table 5. Correlations between parameter variations and changes in methane fluxes are expressed by coloured circles of different sizes. The size of the circle represents the correlation coefficient r^2, with bigger circles showing higher r^2 values, on a nonlinear scale. The colours represent the regression slope, with darker colours indicating steeper slopes and hence a strong increase (red) or decrease (blue) in methane fluxes with increasing parameter value. The parameters on the left influence the production or oxidation of methane and the parameters on the right the transport pathways. The size and colour of the circles are schematic only, hence no scale bars are given.

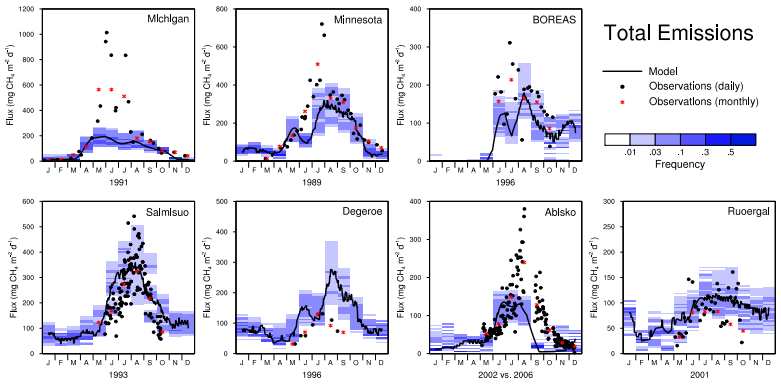

Fig. 5. Modelled methane emissions compared to observations for seven sites. Model results are plotted as 30-day running mean for the best-guess parameter values (black line) and as histograms for each month covering the entire parameter space (blue shading). Observations are plotted as daily values (black dots) and as monthly averages of daily values (red stars). Note that the scale of *y*-axes varies between plots.

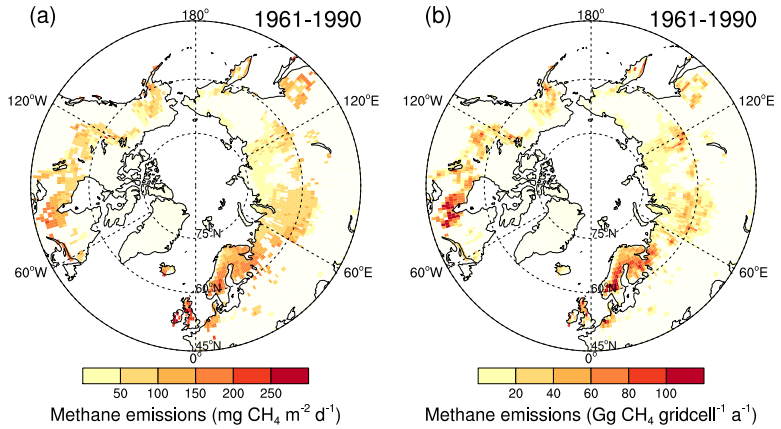

Fig. 6. Methane emissions from the circumpolar region for the period 1961–1990 using the CRU climatology CL 1.0 data to drive LPJ-WHyMe. **(a)** Mean daily methane emissions averaged over the entire year and **(b)** total annual emissions per grid cell. To obtain emissions per grid cell, the fluxes were weighted by the peatland area in each grid cell, by the Prigent scaling factor of 0.38 to adjust for an overestimation of the area and by a scaling factor of 0.75 to account for lower CH_4 emissions from drier sites (see Sect. 6.1 for explanation of these scaling factors).